resorbing activity when they are stimulated by RANKL in the presence of M-CSF, whereas *NFATc1*$^{-/-}$ cells are unable to generate osteoclasts (Fig. 2 D), despite normal development into the monocyte/macrophage lineage (Fig. S4, available at http://www.jem.org/cgi/content/full/jem.20051150/DC1). To investigate the function of NFATc1 and NFATc2 further, we ectopically expressed NFATc1 and NFATc2 under the control of the *LTR* promoter using retrovirus-mediated gene transfer (20) in *NFATc1*$^{-/-}$ osteoclast precursor cells. As expected, the formation of bone-resorbing osteoclasts was rescued by retroviral expression of NFATc1. Surprisingly, osteoclast formation recovered, albeit at a reduced efficiency, as the result of forced expression of NFATc2. This demonstrated that forced expression of NFATc2 compensates for the loss of the *NFATc1* gene (Fig. 2 D).

Selective autoamplification of *NFATc1* during osteoclastogenesis

How can we reconcile the in vivo essential role of *NFATc1* in osteoclastogenesis with the observation that *NFATc1* deficiency is compensated for by forced expression of NFATc2? Whereas NFATc2 is expressed constitutively in BMMs at a low level, mRNA of *NFATc1* is induced selectively and potently by RANKL (5) (Fig. 3 A). The induction of *NFATc1*, but not *NFATc2*, is down-regulated by the calcineurin inhibitor, FK506, which suppresses the activity of NFAT (Fig. 3 A). This suggests that *NFATc1* is autoregulated selectively by NFAT when BMMs are stimulated with RANKL, and that the resulting expression pattern may explain the specificity of *NFATc1*. Although *NFATc1* also is autoregulated in T cells (20, 21), the expression pattern during osteoclastogenesis (autoamplification) is characterized by a monotone increase and magnitude of amplification. Three isoforms (A, B, and C) of NFATc1 are well documented in T cells (20, 22), but it remains to be clarified which isoform is involved in osteoclastogenesis. Using specific PCR primers, we found that mRNA expression of the shortest isoform, NFATc1/A, is induced selectively in RANKL-stimulated BMMs (Fig. 3 B); immunoblot analysis yielded consistent results (Fig. 3 C). Therefore, we investigated the regulatory mechanism of the P1 promoter of the *NFATc1* gene, which regulates NFATc1/A induction (20), in comparison with the *NFATc2* promoter. To determine the transcriptional start site of mouse *NFATc2* gene, a 5′ rapid amplification of cDNA ends experiment was performed. The putative transcription factor binding sites in the 5′ flanking region of the *NFATc1* and *NFATc2* gene are shown in Fig. 3 D. Unexpectedly, these results suggest that not only the *NFATc1* promoter but also the *NFATc2* promoter contain multiple NFAT binding sites.

Recruitment of NFATc1 and other transcription factors to the *NFAT* promoters

Chromatin immunoprecipitation (ChIP) analysis shows that NFATc2 is recruited to the *NFATc1* promoter at the earliest phase of osteoclast differentiation (Fig. 3 E). 24 h after RANKL stimulation, NFATc1 mainly occupies the promoter instead of NFATc2, and c-Fos is concomitantly recruited to the promoter (Fig. 3 E); this is consistent with the strong induction of *NFATc1* at this time point. This occupancy persists during terminal differentiation of osteoclasts, and indicates that autoamplification of *NFATc1* occurs during this process and that c-Fos may contribute to it. This is congruent with the critical role of c-Fos in RANKL-mediated induction of *NFATc1*, which was reported previously (5, 23). NF-κB is activated rapidly by RANKL (24), and a recent study suggests that NF-κB activity is important for RANKL-mediated induction of *NFATc1* at the early phase of osteoclastogenesis (25). Consistent with this, NF-κB components p50 and p65 are recruited to the *NFATc1* promoter 1 h after RANKL stimulation. However, this recruitment is not observed after 24 h (Fig. 3 E), which suggests that NF-κB is important for the initial induction of *NFATc1* in cooperation with NFATc2. Although NFATc2 is detected on the *NFATc1* promoter without RANKL stimulation, *NFATc1* is not induced under this condition, which suggests that additional stimulation, such as NF-κB activation, is important for the efficient triggering of this promoter. This is consistent with the observation in the luciferase assay that the *NFATc1* promoter is not activated fully by NFATc2 alone, but is activated markedly by the coexpression of NFATc2 and NF-κB (Fig. 3 F). The basal calcineurin activity in osteoclast precursor cells may contribute to the nuclear localization of NFATc2 without RANKL addition (Fig. S5, available at http://www.jem.org/cgi/content/full/jem.20051150/DC1). Because osteoclast differentiation was not affected in *NFATc2*$^{-/-}$ mice, the function of NFATc2 evidently can be compensated by other factors, although it may contribute to physiologic regulation of the initial induction of *NFATc1*. A reporter plasmid that is driven by the *NFATc1*-P1 promoter, but not by the *NFATc2* promoter, is activated markedly by NFAT in cooperation with NF-κB (Fig. 3 F). These results indicate that the *NFATc1* promoter is distinct from the *NFATc2* promoter in that the former is exclusively under autoregulation by NFAT; this further suggests that an autoregulatory mechanism contributes to the essential role of *NFATc1*.

Epigenetic regulation of *NFATc1* gene determines its unique spatiotemporal induction pattern during osteoclastogenesis

To gain insight into the selective recruitment of NFATc1 to the *NFATc1* promoter, we examined the association of transcriptional cofactors with these promoters. *NFATc1* promoter is associated increasingly with transcriptional coactivators with histone acetylase activity, such as CREB-binding protein (CBP) and p300/CBP-associated factor (PCAF), but is dissociated with histone deacetylase 1 (HDAC1; Fig. 4 A). It is notable that histone acetylation in the *NFATc1* promoter increased gradually after RANKL stimulation and that the high acetylation status was sustained, but this was not observed in the *NFATc2* promoter (Fig. 4 B). Methylation of histone H3 lysine 4, which is characteristic of the transcriptionally active locus, is up-regulated exclusively in the *NFATc1* promoter (Fig. 4 B). Conversely, the *NFATc2* promoter is associated con-

Downloaded from www.jem.org on February 22, 2006

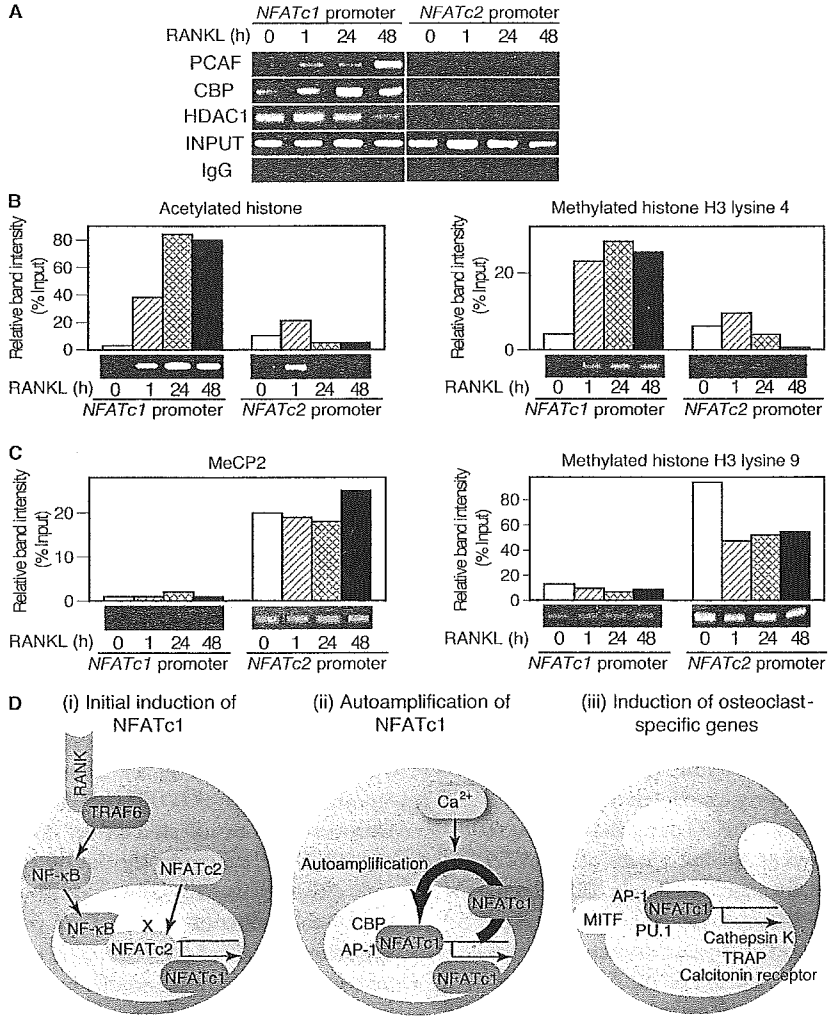

Figure 4. Epigenetic regulation of *NFATc1* promoter underlies the selective autoamplification of *NFATc1*. (A) Analysis of chromatin modification–related factors in *NFATc1* and *NFATc2* promoters by ChIP in RANKL-stimulated BMMs during osteoclastogenesis. (B) ChIP assay for acetylated histone and methylated histone H3 lysine 4. (C) ChIP assay for MeCP2 and methylated histone H3 lysine 9. (D) A schematic diagram of three stages of osteoclast differentiation that are governed by NFATc1. (i) NFATc2 is recruited to the *NFATc1* promoter at the very early phase, but this is not enough to activate the *NFATc1* promoter. The binding of RANKL to receptor activator of NF-κB (RANK) results in the recruitment of TNF receptor–associated factor (TRAF) 6, and leads to the activation of downstream molecules, such as NF-κB (25, 34). Cooperation of NFATc2 and NF-κB activates the initial induction of *NFATc1*, but because *NFATc2*-deficient mice have no obvious defect in osteoclast differentiation, unknown factor(s) (shown as X) may compensate for the loss of *NFATc2* in these mice. (ii) RANKL–RANK interaction cooperates with immunoreceptors to activate the calcium signals (28), which stimulate the NFATc1 activation by way of calcineurin (5). NFATc1 bind to its own promoter, which leads to the robust induction of *NFATc1*; AP-1 (containing c-Fos) is critical for this autoamplification. Selective recruitment of NFATc1 to the promoter of *NFATc1*, but not *NFATc2*, is explained in part, by epigenetic regulation. (iii) Several osteoclast-specific genes, such as *cathepsin K*, *TRAP*, and *calcitonin receptor*, are activated by a transcriptional complex that contains NFATc1 and other cooperators, such as AP-1, PU.1, and microphthalmia-associated transcription factor (MITF).

stantly with methylated DNA-binding proteins, such as the methyl-CpG binding protein 2 (MeCP2) (Fig. 4 C), which suggests that the *NFATc2* promoter specifically is silenced during osteoclast differentiation. Consistent with this notion, we detected high levels of methylated histone H3 lysine 9 only in the *NFATc2* promoter (Fig. 4 C). These results suggest that epigenetic regulation underlies the specific autoamplification of *NFATc1*.

DISCUSSION

Our results illustrate that the essential importance of a gene is not only attributable to the specific biochemical function of the coded protein, but also is determined epigenetically by the distinct regulatory mechanism of gene expression. The role of *GATA-1* and *GATA-3* in erythropoiesis and Th2 cell differentiation are examples in which the essential importance of one member of a group of structurally related pro-

Downloaded from www.jem.org on February 22, 2006

teins of interchangeable function is based on an autoregulatory mechanism (26, 27). These studies suggest that autoregulation of transcription factors is one of the critical mechanisms for cell fate determination (2). In a future study, generation of mice with an *NFATc2* knock-in into the *NFATc1* locus will be an intriguing strategy to provide the conclusive in vivo evidence.

As depicted in Fig. 4 D, in the differentiation of osteoclasts, preexisting NFATc2 cooperates with other RANKL-stimulated transcription factors, such as NF-κB, to activate the initial induction of *NFATc1*, followed by an autoamplification phase of *NFATc1*. It was reported that the activator protein (AP)–1 component, c-Fos, is critical for RANKL-mediated induction of *NFATc1* (5, 23). Consistent with this, c-Fos is recruited selectively to the *NFATc1* promoter at the autoamplification phase (Fig. 3 E). The composite NFAT/AP-1 site is observed exclusively in the *NFATc1* promoter (Fig. 3 D) (20). This lends further support to the notion that the cooperation of NFAT and AP-1 is responsible for the specific activation of the *NFATc1* promoter and its autoamplification.

Calcium signal-mediated activation of NFATc1 also triggers the autoamplification loop of *NFATc1* and ensures a sustained *NFATc1*-dependent transcriptional program (5, 28) in which osteoclast-specific genes are activated by a transcriptional complex that involves NFATc1, AP-1, and other cooperators (5, 29). Accumulating evidence indicates that NFATc1 regulates many osteoclast-specific genes, such as *cathepsin K* (29), *TRAP* (5, 30), *calcitonin receptor* (5, 30), and *osteoclast-associated receptor* (30), in cooperation with other transcription factors (e.g., PU.1 and microphthalmia-associated transcription factor), although the components of the transcriptional complex are not always the same (30) (Fig. 4 D, iii). A distinct pattern of calcium oscillation, which efficiently keeps NFATc1 transcriptionally active in the nucleus (31), may explain the specific spaciotemporal expression of NFATc1 in the osteoclast lineage (5), in contrast to T cells. FK506 inhibited osteoclast formation, even when it was added at the late phase of osteoclastogenesis (48–72 h after RANKL stimulation, unpublished data); this suggests that calcium signaling is also critical for the autoamplification of *NFATc1*.

Successful application of FLC transfer and blastocyst complementation, first established in the immune system, provided genetic evidence that *NFATc1* is essential for osteoclast differentiation and maintenance of the skeletal system. Modulation of the *NFATc1* autoamplification pathway has promise as a strategy for suppressing the excessive osteoclast formation that is characteristic of a variety of bone diseases.

MATERIALS AND METHODS

Mice and analysis of bone phenotype. Generation of $Fos^{-/-}$ and $NFATc1^{-/-}$ mice has been described previously (8, 13). *NFATc2* mice (17) were provided by L.H. Glimcher (Harvard Medical School, Boston, MA). Histologic, histomorphometric, and microradiographic examinations were performed using essentially the same methods as described (32). Statistical analysis was performed using Student's *t* test. All mice were kept in a specific pathogen-free environment, and all animal experiments were performed with the approval of the institutional committee of Tokyo Medical and Dental University.

In vitro osteoclastogenesis and retroviral gene transfer. Bone marrow cells or FLCs were cultured in α-MEM (GIBCO BRL) containing 10% FBS (Sigma-Aldrich) and 10 ng ml^{-1} M-CSF (R&D Systems). After 2 d, adherent cells were used as osteoclast precursor cells. In osteopetrotic mice, osteoclast precursor cells were obtained similarly from splenocytes. We described the method of RANKL-induced in vitro osteoclastogenesis, retroviral gene transfer, characterization of osteoclasts, and immunostaining (5, 24, 32). All data are expressed as mean ± SEM ($n = 6$). Retroviral vectors, pEGZ-NFATc1/A (NFATc1 virus) and pEGZ-NFATc2 (NFATc2 virus), were described previously (20), and infection efficiencies of both retrovirus vectors into osteoclast precursor cells were ~40%, as described previously (24).

Fetal liver cell transfer. $NFATc1^{-/-}$ and $NFATc1^{+/-}$ embryos were obtained by crossing $NFATc1^{+/-}$ parental mice. Total liver cells (10^7 cells) from embryonic day (E) 13.5 embryos were injected into the liver of recipient $Fos^{-/-}$ newborn (2 d) mice, which were analyzed at 6 wk of age. The recipient mice were treated with busulfan (Sigma-Aldrich) in utero by i.p. administration to pregnant mice (12.5 mg kg^{-1}) twice at 17.5 and 18.5 d postcoitum.

$Fos^{-/-}$ blastocyst complementation. Establishment of $NFATc1^{-/-}$ ES cell lines has been described (33). $NFATc1^{-/-}$ ES cells or wild-type ES cells (E14K) were injected into E3.5 $Fos^{-/-}$ blastocysts that were obtained by fertilizing $Fos^{-/-}$ gametes from $Fos^{-/-}$ paternal and maternal mice using in vitro fertilization technique. Resultant blastocysts were transferred to pseudopregnant foster mothers to generate chimeric mice.

RT-PCR and GeneChip analysis. RNA extraction, semiquantitative RT-PCR, and GeneChip analysis were performed as described previously (5, 32). The following PCR primers were used to detect NFAT isoforms. NFATc1/A: 5′-GGTAACTCTGTCTTTCTAACCTTAAGCTC-3′ (sense) and 5′-GTGATGACCCCAGCATGCACCAGTCACAG-3′ (antisense); NFATc1/B: 5′-CCCATCCGCCAGGCTACAGCCGCAGTAA-3′ (sense) and 5′-TTCGGTAAGTTGGGATTTCTGAGTGGTACC-3′ (antisense); NFATc1/C: 5′-CCCATCCGCCAGGCTACAGCCGCAGTAA-3′ (sense) and 5′-TGAGTGGTACCAGATGTGGGTCCAGTTTAT-3′ (antisense).

Chromatin immunoprecipitation. ChIP was performed with the ChIP Assay Kit (Upstate Biotechnology) according to the manufacturer's instructions, using antibodies against NFATc1, NFATc2, p300/CBP-associated factor, histone deacetylase 1, p50, CBP, MeCP2 (Santa Cruz Biotechnology, Inc.), p65, acetylated histone, mono/di/trimethyl-histone H3 lysine 4, dimethyl-histone H3 lysine 9 (Upstate Biotechnology), c-Fos (Calbiochem), and normal IgG (Santa Cruz Biotechnology, Inc.). The purified DNA was analyzed by PCR using primers that detect sequences containing the *NFATc1*-P1 promoter: 5′-CCGGGACGCCCATGCAATCTGTTAGTAATT-3′ (sense) and 5′-GCGGGTGCCCTGAGAAAGCTACTCTCCCTT-3′ (antisense) and the *NFATc2* promoter: 5′-TTATCAGGGAGCACTGCCCATCTCCGCTTT-3′ (sense) and 5′-CGGTCTGGCCTGAGCGACAGGCCCAGACAA-3′ (antisense).

Luciferase reporter gene assay. The reporter plasmid pNFATc1P1-0.8 kb-luc (pNFATc1-pr-luc) was described previously (20). pNFATc2-0.8 kb-luc (pNFATc2-pr-luc) was constructed by inserting a 0.8-kb NheI–XhoI fragment of the mouse *NFATc2* promoter into the same sites of the pGL3 basic promoter vector (Promega). The mouse *NFATc2* promoter region was amplified by PCR using following primers: 5′-GCTAGCTGTTTTGGTGACTGTTATCATGCTGGG-3′ (sense) and 5′-CTCGAGCTTCCTGCTCAAGGCACCTGTTGCAG-3′ (antisense). Transfection into HEK293T cells and measurement of luciferase activity were performed as described (5) using the Dual-luciferase reporter assay system (Promega).

Downloaded from www.jem.org on February 22, 2006

Online supplemental material. Fig. S1 shows the gain-of-function analyses of *NFATc1* and *NFATc2* in osteoclasts. Fig. S2 shows the histomorphometric evaluation of osteoclasts in *NFATc2*$^{-/-}$ mice. Fig. S3 shows the normal osteoclast differentiation and expression of NFATc1 in *NFATc2*$^{-/-}$ monocyte/macrophage precursor cells that were stimulated with RANKL/M-CSF. Fig. S4 shows the development into the monocyte/macrophage lineage from *NFATc1*$^{-/-}$ FLCs. Fig. S5 shows the effect of FK506 on the recruitment of NFATc2 to the *NFATc1* promoter without RANKL stimulation. Also, details of the methods for phylogenetic tree analysis and 5′ rapid amplification of cDNA ends analysis are available. Online supplemental material is available at http://www.jem.org/cgi/content/full/jem.20051150/DC1.

We are grateful to L.H. Glimcher for the mice. We thank T. Taniguchi, S. Mori, H. Endo, T. Watanabe, N. Yoshida, K. Aoki, T. Ishida, H. Murayama, M. Tsujimoto, M. Isobe, S. Kamano, T. Honda, T. Koga, S. Harumiya, J. Hirooka, A. Suematsu, Y. Kim, K. Nishikawa, H.J. Gober, N. Kumasaki, H. Takatsuna, Y. Morishita, T. Yokochi, M.A. Hayashi, and I. Kawai for discussion and technical assistance.

This work was supported in part by the Precursory Research for Embryonic Science and Technology and Solution Oriented Research for Science and Technology programs of the Japan Science and Technology Agency; grants for the Genome Network Project from Ministry of Education, Culture, Sports, Science, and Technology of Japan (MEXT); grants for the 21st century Center of Excellence program; grants-in-aid for Scientific Research from the Japan Society for the Promotion of Science and MEXT; Health Sciences Research Grants from the Ministry of Health, Labor and Welfare of Japan; and grants from the Mitsubishi Foundation, The Kato Trust for Nambyo Research, Takeda Science Foundation, Daiwa Securities Health Foundation, The Naito Foundation, Kowa Life Science Foundation, Suzuken Memorial Foundation, Kato Memorial Bioscience Foundation, Cell Science Research Foundation, and Uehara Memorial Foundation. The work in E. Serfling's laboratory was supported by the German Research Foundation, the Wilhelm-Sander Foundation, and the Scheel Foundation for Cancer Research.

The authors have no conflicting financial interests.

Submitted: 7 June 2005
Accepted: 13 September 2005

REFERENCES

1. Crabtree, G.R., and E.N. Olson. 2002. NFAT signaling: choreographing the social lives of cells. *Cell.* 109(Suppl):S67–79.
2. Hogan, P.G., L. Chen, J. Nardone, and A. Rao. 2003. Transcriptional regulation by calcium, calcineurin, and NFAT. *Genes Dev.* 17: 2205–2232.
3. Peng, S.L., A.J. Gerth, A.M. Ranger, and L.H. Glimcher. 2001. NFATc1 and NFATc2 together control both T and B cell activation and differentiation. *Immunity.* 14:13–20.
4. Teitelbaum, S.L., and F.P. Ross. 2003. Genetic regulation of osteoclast development and function. *Nat. Rev. Genet.* 4:638–649.
5. Takayanagi, H., S. Kim, T. Koga, H. Nishina, M. Isshiki, H. Yoshida, A. Saiura, M. Isobe, T. Yokochi, J. Inoue, et al. 2002. Induction and activation of the transcription factor NFATc1 (NFAT2) integrate RANKL signaling in terminal differentiation of osteoclasts. *Dev. Cell.* 3:889–901.
6. Theill, L.E., W.J. Boyle, and J.M. Penninger. 2002. RANK-L and RANK: T cells, bone loss, and mammalian evolution. *Annu. Rev. Immunol.* 20:795–823.
7. Ikeda, F., R. Nishimura, T. Matsubara, S. Tanaka, J. Inoue, S.V. Reddy, K. Hata, K. Yamashita, T. Hiraga, T. Watanabe, et al. 2004. Critical roles of c-Jun signaling in regulation of NFAT family and RANKL-regulated osteoclast differentiation. *J. Clin. Invest.* 114:475–484.
8. de la Pompa, J.L., L.A. Timmerman, H. Takimoto, H. Yoshida, A.J. Elia, E. Samper, J. Potter, A. Wakeham, L. Marengere, B.L. Langille, et al. 1998. Role of the NF-ATc transcription factor in morphogenesis of cardiac valves and septum. *Nature.* 392:182–186.
9. Ranger, A.M., M.J. Grusby, M.R. Hodge, E.M. Gravallese, F.C. de la Brousse, T. Hoey, C. Mickanin, H.S. Baldwin, and L.H. Glimcher. 1998. The transcription factor NF-ATc is essential for cardiac valve formation. *Nature.* 392:186–190.
10. Shinkai, Y., G. Rathbun, K.P. Lam, E.M. Oltz, V. Stewart, M. Mendelsohn, J. Charron, M. Datta, F. Young, A.M. Stall, and F.W. Alt. 1992. RAG-2-deficient mice lack mature lymphocytes owing to inability to initiate V(D)J rearrangement. *Cell.* 68:855–867.
11. Mombaerts, P., J. Iacomini, R.S. Johnson, K. Herrup, S. Tonegawa, and V.E. Papaioannou. 1992. RAG-1-deficient mice have no mature B and T lymphocytes. *Cell.* 68:869–877.
12. Wang, Z.Q., C. Ovitt, A.E. Grigoriadis, U. Mohle-Steinlein, U. Ruther, and E.F. Wagner. 1992. Bone and haematopoietic defects in mice lacking c-fos. *Nature.* 360:741–745.
13. Grigoriadis, A.E., Z.Q. Wang, M.G. Cecchini, W. Hofstetter, R. Felix, H.A. Fleisch, and E.F. Wagner. 1994. c-Fos: a key regulator of osteoclast-macrophage lineage determination and bone remodeling. *Science.* 266:443–448.
14. Chen, J., R. Lansford, V. Stewart, F. Young, and F.W. Alt. 1993. RAG-2-deficient blastocyst complementation: an assay of gene function in lymphocyte development. *Proc. Natl. Acad. Sci. USA.* 90:4528–4532.
15. Ho, S.N., D.J. Thomas, L.A. Timmerman, X. Li, U. Francke, and G.R. Crabtree. 1995. NFATc3, a lymphoid-specific NFATc family member that is calcium-regulated and exhibits distinct DNA binding specificity. *J. Biol. Chem.* 270:19898–19907.
16. Graef, I.A., J.M. Gastier, U. Francke, and G.R. Crabtree. 2001. Evolutionary relationships among Rel domains indicate functional diversification by recombination. *Proc. Natl. Acad. Sci. USA.* 98:5740–5745.
17. Hodge, M.R., A.M. Ranger, F. Charles de la Brousse, T. Hoey, M.J. Grusby, and L.H. Glimcher. 1996. Hyperproliferation and dysregulation of IL-4 expression in NF-ATp–deficient mice. *Immunity.* 4:397–405.
18. Ranger, A.M., L.C. Gerstenfeld, J. Wang, T. Kon, H. Bae, E.M. Gravallese, M.J. Glimcher, and L.H. Glimcher. 2000. The nuclear factor of activated T cells (NFAT) transcription factor NFATp (NFATc2) is a repressor of chondrogenesis. *J. Exp. Med.* 191:9–22.
19. Koga, T., Y. Matsui, M. Asagiri, T. Kodama, B. de Crombrugghe, K. Nakashima, and H. Takayanagi. 2005. NFAT and Osterix cooperatively regulate bone formation. *Nat. Med.* 11:880–885.
20. Chuvpilo, S., E. Jankevics, D. Tyrsin, A. Akimzhanov, D. Moroz, M.K. Jha, J. Schulze-Luehrmann, B. Santner-Nanan, E. Feoktistova, T. Konig, et al. 2002. Autoregulation of NFATc1/A expression facilitates effector T cells to escape from rapid apoptosis. *Immunity.* 16:881–895.
21. Zhou, B., R.Q. Cron, B. Wu, A. Genin, Z. Wang, S. Liu, P. Robson, and H.S. Baldwin. 2002. Regulation of the murine *Nfatc1* gene by NFATc2. *J. Biol. Chem.* 277:10704–10711.
22. Chuvpilo, S., M. Zimmer, A. Kerstan, J. Glockner, A. Avots, C. Escher, C. Fischer, I. Inashkina, E. Jankevics, F. Berberich-Siebelt, et al. 1999. Alternative polyadenylation events contribute to the induction of NF-ATc in effector T cells. *Immunity.* 10:261–269.
23. Matsuo, K., D.L. Galson, C. Zhao, L. Peng, C. Laplace, K.Z. Wang, M.A. Bachler, H. Amano, H. Aburatani, H. Ishikawa, and E.F. Wagner. 2004. Nuclear factor of activated T-cells (NFAT) rescues osteoclastogenesis in precursors lacking c-Fos. *J. Biol. Chem.* 279:26475–26480.
24. Takayanagi, H., K. Ogasawara, S. Hida, T. Chiba, S. Murata, K. Sato, A. Takaoka, T. Yokochi, H. Oda, K. Tanaka, et al. 2000. T-cell-mediated regulation of osteoclastogenesis by signalling cross-talk between RANKL and IFN-γ. *Nature.* 408:600–605.
25. Takatsuna, H., M. Asagiri, T. Kubota, K. Oka, T. Osada, C. Sugiyama, H. Saito, K. Aoki, K. Ohya, H. Takayanagi, and K. Umezawa. 2005. Inhibition of RANKL-induced osteoclastogenesis by (-)-DHMEQ, a novel NF-κB Inhibitor, through downregulation of NFATc1. *J. Bone Miner. Res.* 20:653–662.
26. Takahashi, S., R. Shimizu, N. Suwabe, T. Kuroha, K. Yoh, J. Ohta, S. Nishimura, K.C. Lim, J.D. Engel, and M. Yamamoto. 2000. GATA factor transgenes under GATA-1 locus control rescue germline GATA-1 mutant deficiencies. *Blood.* 96:910–916.
27. Ouyang, W., M. Lohning, Z. Gao, M. Assenmacher, S. Ranganath, A. Radbruch, and K.M. Murphy. 2000. Stat6-independent GATA-3 autoactivation directs IL-4–independent Th2 development and commitment. *Immunity.* 12:27–37.
28. Koga, T., M. Inui, K. Inoue, S. Kim, A. Suematsu, E. Kobayashi, T.

Downloaded from www.jem.org on February 22, 2006

Iwata, H. Ohnishi, T. Matozaki, T. Kodama, et al. 2004. Costimulatory signals mediated by the ITAM motif cooperate with RANKL for bone homeostasis. *Nature.* 428:758–763.
29. Matsumoto, M., M. Kogawa, S. Wada, H. Takayanagi, M. Tsujimoto, S. Katayama, K. Hisatake, and Y. Nogi. 2004. Essential role of p38 mitogen-activated protein kinase in cathepsin K gene expression during osteoclastogenesis through association of NFATc1 and PU.1. *J. Biol. Chem.* 279:45969–45979.
30. Kim, Y., K. Sato, M. Asagiri, I. Morita, K. Soma, and H. Takayanagi. 2005. Contribution of NFATc1 to the transcriptional control of immunoreceptor OSCAR but not TREM-2 during osteoclastogenesis. *J. Biol. Chem.* 280:32905–32913.
31. Tomida, T., K. Hirose, A. Takizawa, F. Shibasaki, and M. Iino. 2003. NFAT functions as a working memory of Ca^{2+} signals in decoding Ca^{2+} oscillation. *EMBO J.* 22:3825–3832.
32. Takayanagi, H., S. Kim, K. Matsuo, H. Suzuki, T. Suzuki, K. Sato, T. Yokochi, H. Oda, K. Nakamura, N. Ida, et al. 2002. RANKL maintains bone homeostasis through c-Fos–dependent induction of *interferon-β*. *Nature.* 416:744–749.
33. Yoshida, H., H. Nishina, H. Takimoto, L.E. Marengere, A.C. Wakeham, D. Bouchard, Y.Y. Kong, T. Ohteki, A. Shahinian, M. Bachmann, et al. 1998. The transcription factor NF-ATc1 regulates lymphocyte proliferation and Th2 cytokine production. *Immunity.* 8:115–124.
34. Takayanagi, H. 2005. Mechanistic insight into osteoclast differentiation in osteoimmunology. *J. Mol. Med.* 83:170–179.

Downloaded from www.jem.org on February 22, 2006

J. Biochem. **137**, 423–430 (2005)
DOI: 10.1093/jb/mvi046

Novel Role of the Small GTPase Rheb: Its Implication in Endocytic Pathway Independent of the Activation of Mammalian Target of Rapamycin

Kota Saito, Yasuhiro Araki, Kenji Kontani, Hiroshi Nishina and Toshiaki Katada*

Department of Physiological Chemistry, Graduate School of Pharmaceutical Sciences, University of Tokyo, 7-3-1 Hongo, Bunkyo-ku, Tokyo 113-0033

Received January 8, 2005; accepted February 1, 2005

The Ras-homologous GTPase Rheb that is conserved from yeast to human appears to be involved not only in cell growth but also in nutrient uptake. Recent biochemical analysis revealed that tuberous sclerosis complex (TSC), a GTPase-activating protein (GAP), deactivates Rheb and that phosphatidylinositol 3′-kinase (PI3k)-Akt/PKB kinase pathway activates Rheb through inhibition of the GAP-mediated deactivation. Although mammalian target of rapamycin (mTOR) kinase is implicated in the downstream target of Rheb, the direct effector(s) and exact functions of Rheb have not been fully elucidated. Here we identified that Rheb expression in cultured cells induces the formation of large cytoplasmic vacuoles, which are characterized as late endocytic (late endosome- and lysosome-like) components. The vacuole formation required the GTP form of Rheb, but not the activation of the downstream mTOR kinase. These results suggest that Rheb regulates endocytic trafficking pathway independent of the previously identified mTOR pathway. The physiological roles of the two Rheb-dependent signaling pathways are discussed in terms of nutrient uptake and cell growth or cell cycle progression.

Key words: late endosome, lysosome, mTOR, Rheb, small GTPase.

Abbreviations: DMEM, Dulbecco's modified Eagle's minimum essential medium; GAP, GTPase-activating protein; mTOR, mammalian target of rapamycin; PI3k, phosphatidylinositol 3′-kinase; Rheb, *ras* homologue enriched in brain; TSC, tuberous sclerosis complex.

Members of the small GTPase Ras superfamily act as molecular switches that regulate a wide range of cellular functions including cell proliferation and differentiation. Ras homologue enriched in brain, Rheb, is a member of an atypical family of Ras-related G proteins, of which sequences in the GTP-binding domain have not been conserved (*1*). Di-Ras1, Di-Ras2, and ARHI also belong to the atypical GTPase family (*2*). Rheb was initially identified as a gene whose mRNA expression is increased in rat brain by seizures or by the stimulation of long-term potentiation (*3*). Recently, Rheb has received significant attention, since it was identified as a positive regulator of the mammalian target of rapamycin (mTOR) pathway, which regulates cell growth in response to various growth factors, cellular energy and nutrient levels (*4–10*). Moreover, the TSC1/TSC2 complex, of which mutations leads to tuberous sclerosis complex (TSC), was found to be a GTPase-activating protein (GAP) for Rheb (*5–8*, *11*).

From recent biochemical studies in mammalian cells, Rheb-related signaling pathways leading to cell growth may be summarized as follows. The stimulation of growth factor receptors at the cell surface results in the activation of phosphatidylinositol 3′-kinase (PI3k), which then phosphorylates Akt/PKB (*12*, *13*). The activated Akt phosphorylates TSC2 to negatively regulate its GAP activity toward Rheb (*6*, *14*, *15*). This results in the accumulation of GTP-Rheb and stimulates the mTOR kinase activity (*4–10*). Phosphorylation of p70 ribosomal S6 kinase (S6K) and the translation initiation factor 4E-BP1, which are responsible for the increase in protein synthesis, has been implicated in the downstream events of mTOR kinase (*16*, *17*). Thus, Rheb is involved in the signaling pathways responsible for cell growth and cell cycle progression.

On the other hand, Rheb appears to play an important role in intracellular uptake of nutrients such as amino acids. Rheb is conserved from yeast to human, and recent genetic studies have contributed significantly to the understanding of its function. In yeast, arginine uptake was regulated positively and negatively by TSC and Rheb, respectively (*18–20*). In addition, Tsc1 and Tsc2 knockouts in *Schizosaccaromyces pombe* exhibited abnormal intracellular distribution of an amino-acid permease (*21*). In human, TSC patients suffer from seizures and epilepsy, which may be related to the dysfunction of extracellular glutamate uptake in glial cells. The accumulated glutamate in the synaptic cleft may cause neuronal cell death. However, the linkage between Rheb activation and nutrient uptake and the molecular mechanism underlying TSC epileptogenesis have not been fully clarified.

In the present study, we found that Rheb activation induces the formation of large vacuoles in the cytoplasm

*To whom correspondence may be addressed. Tel: +81-3-5841-4750, Fax: +81-3-5841-4751, E-mail: katada@mol.f.u-tokyo.ac.jp

© 2005 The Japanese Biochemical Society.

of Rheb-transfected cells, and that the vacuoles are characterized as late endosome- or lysosome-like organelles. The large vacuole formation was dependent on the GTPase cycle of Rheb and suppressed by inhibition of the PI3k activity. However, inhibition of mTOR kinase did not affect the Rheb-induced vacuole formation. These results suggest that Rheb plays an important role in endocytic trafficking pathway independent of the previously identified mTOR pathway that leads to cell growth and cell-cycle progression. Possible roles of Rheb are discussed in terms of the relationship between the Rheb-dependent endocytic pathway and nutrient uptake.

MATERIALS AND METHODS

Northern Blot Analysis—Expression patterns of Rheb and Rheb2 mRNAs were analyzed using human multiple tissue membranes (BD Biosciences). Full-length sequences of Rheb and Rheb2 that had been radiolabeled with [α-^{32}P]dCTP were hybridized to the membranes overnight at 65°C in the Expresshyb solution (BD Biosciences), and the membranes were subjected to autoradiography (*22*).

Cell Culture and Transfection—MDCK, HeLa, 1321N1, and 293 cells were maintained in Dulbecco's modified Eagle's minimum essential medium (DMEM) supplemented with 10% fetal bovine serum. The cells cultured in a 35-mm dish were transfected with 1 μg of DNA and 2 μl of LipofectAMINE 2000 (Invitrogen) in Opti-MEM according to the manufacturer's protocol and incubated at 37°C for 16 h unless otherwise specified.

Confocal Microscopic Analysis—The transfected cells in a glass-based dish (35-mm diameter, Matsunami) were analyzed by Carl Zeiss confocal microscopy with LSM510 (*23*). For the analysis of dextran uptake and the labeling of acidic organelles (see Fig. 4), the transfected MDCK cells were further incubated at 37°C with 1 mg/ml of FITC-dextran (Molecular Probes) for 12 h (Fig. 4A) and 50 nM Lysotracker Green (Molecular Probes) for 1 h (Fig. 4B), then washed for four times with PBS before the confocal microscopic analysis. In some experiments (see Fig. 4C), MDCK cells were first incubated with 1 mg/ml of FITC-dextran in DMEM at 37°C for 4 h and further cultured without the dextran for an additional 20 h. The dextran-preloaded cells were transfected with Dsred-Rheb and incubated for the indicated times before the confocal microscopic analysis.

Analysis of Akt Kinase Activity—293 cells cultured in a 6-cm dish were transfected with 1.5 μg of Myc-Akt and 1.5 μg of FLAG or FLAG-Rheb and further incubated in the presence or absence of 50 μM LY294002 (Calbiochem) for 16 h. The cells were solubilized with an extraction buffer consisting of 40 mM Na-Hepes (pH 7.4), 75 mM NaCl, 1% Triton X-100, 1 mM EDTA, 15 mM NaF, 1 mM Na_3VO_4, 10 mM $Na_4P_2O_7$, 1 μg/ml leupeptin, and 2 μg/ml aprotinin, and the cell lysate was immunoprecipitated with Myc-antibody (Sigma) conjugated to Protein G-agarose (Amersham Biosciences). The immunocomplexes were washed three times with a buffer consisting of 50 mM Na-Hepes, 100 mM NaCl, 0.2% Triton X-100, 15 mM NaF, 1 mM Na_3VO_4, 10 mM $Na_4P_2O_7$, 4 mM EDTA, 1 mM DTT, and 2 μg/ml aprotinin, then twice with a kinase buffer consisting of 50 mM Na-Hepes, 0.01% Triton X-100, 1 mM DTT, 10 mM $MgCl_2$. They were then incubated with the kinase buffer further supplemented with 50 μM ATP, 3 μCi [γ-^{32}P]ATP, and 10 μg/ml of GST-GSK3β at 37°C for 20 min. Phosphorylated proteins were analyzed by SDS-PAGE, and the radioactivity was visualized with a BAS-1800 bioimaging analyzer (Fuji Firm).

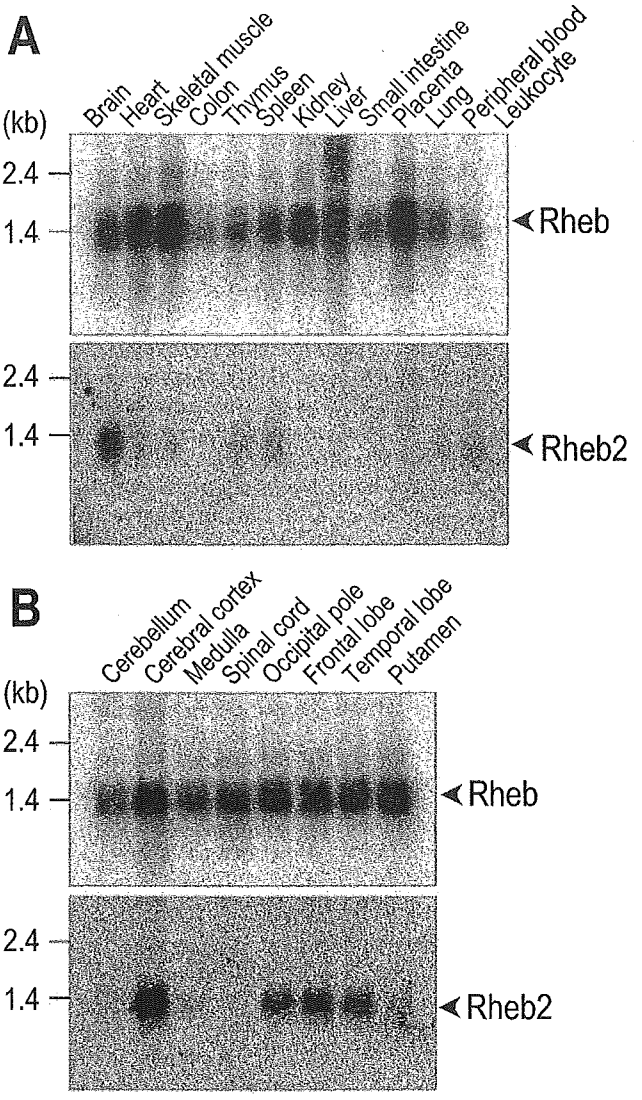

Fig. 1. **Northern blot analysis of Rheb and Rheb2.** Membranes blotted with RNAs obtained from various human tissues (A) and the brain regions (B) were hybridized with ^{32}P-labeled Rheb (top panels) and Rheb2 (bottom panels) probes, respectively, as described under "MATERIALS AND METHODS."

Analysis of mTOR Kinase Activity—293 cells in a 6-cm dish were transfected with 1.5 μg of HA-S6K and 1.5 μg of FLAG or FLAG-Rheb and further incubated in the presence or absence of 40 nM rapamycin (Calbiochem) for 5 h. The cells were washed with PBS and further cultured in DMEM supplemented with 0.1% BSA in the presence or absence of rapamycin for additional 12 h. The cells were solubilized with the extraction buffer, and the cell lysate was immunoprecipitated with anti-HA affinity

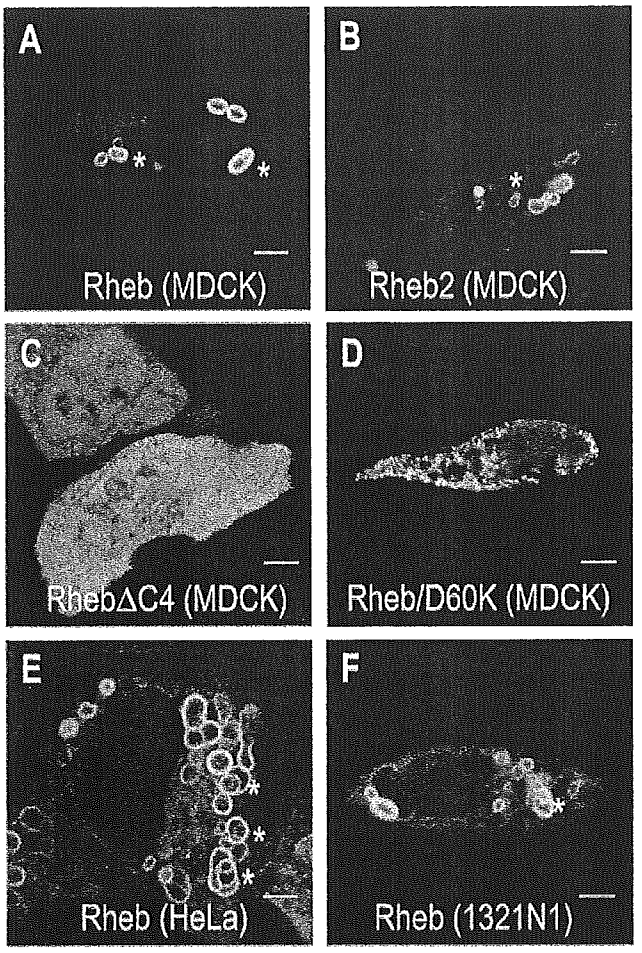

Fig. 2. **Rheb and Rheb2 induce large vacuole formation.** MDCK cells were transfected with EGFP-Rheb (A), EGFP-Rheb2 (B), EGFP-RhebΔC4 (C), or EGFP-Rheb/D60K (D) and cultured for 16 h. HeLa (E) and 1321N1 astrocytoma (F) cells were also transfected with EGFP-Rheb. These cells were analyzed by a confocal microscopy as described under Experimental Procedures. Scale bars indicate 5 μm, and asterisks show the multi-lamellar and multi-vesicular structures.

matrix (Roche). The immunocomplexes were washed five times with a buffer consisting of 20 mM Tris-HCl (pH 7.5), 2 mM EDTA, 100 mM NaCl, and 0.4% Triton X-100, and the precipitated proteins were subjected to SDS-PAGE and Western blotting with anti-p70 (Santa Cruz Biotechnology) and anti-phosphorylated p70 (Cell Signaling) S6K antibodies.

All experiments were repeated at least three times with different batches of the cell samples, and the results were fully reproducible. Hence, most of the data shown are representative of several independent experiments.

RESULTS AND DISCUSSION

Rheb and Rheb2 mRNAs Are Differently Distributed in Human Tissues—In addition to Rheb (Rheb1), human Rheb2 cDNA was recently identified (*4*). To investigate the distribution patterns of Rheb and Rheb2 mRNAs in various human tissues, Northern blot analysis was performed with a radiolabeled probe containing full-length sequences of Rheb and Rheb2. As shown in Fig. 1A, a 1.6-kb Rheb transcript was observed in various human tissues in accordance with a previous report (*3*). In contrast, a 1.6-kb Rheb2 transcript was observed predominantly in the brain and less in the spleen and peripheral blood. Because of the highly sequence homology between Rheb and Rheb2 mRNAs, the specificity of each probe was confirmed by the following analysis. Nitrocellulose membranes were blotted with Rheb and Rheb2 plasmids and hybridized with both probes. Specific signals were observed only when their RNAs were hybridized with the corresponding probes (data not shown). Thus, no cross-hybridization between Rheb and Rheb2 was detected under the present conditions. We next examined the distributions of Rheb and Rheb2 mRNAs in specific brain regions. Rheb was found to be expressed in all brain regions, while Rheb2 mRNA was restricted to the cerebral cortex, occipital pole, frontal and temporal lobes (Fig. 1B). Rheb2 is present only in mammalian cells, although Rheb is highly conserved among various species. Thus, Rheb2 may have a specific role in the brain region of higher eukaryotes, of which activation might lead to epilepsy, which is a typical pathology of TSC patients.

Rheb Induces Large Vacuole Formation—To determine the intracellular localization of Rheb and Rheb2 in living cells, EGFP-tagged proteins were expressed in MDCK cells, and their distributions were analyzed by confocal microscopy (Fig. 2, A–D). Interestingly, the expression of Rheb and Rheb2 induced the formation of large vacuoles dispersed throughout the cells, and the proteins localized to the vacuole membranes (see panels A and B). In contrast, the expression of a mutant Rheb, RhebΔC4, which lacks the carboxy-terminal membrane-anchoring sequence CAAX, give rise to diffused signals and did not induce such large vacuoles (Fig. 2C). Enlarged vacuoles were also induced upon the expression of EGFP-tagged Rheb in HeLa, 1321N1 human astrocytoma cells (Fig. 2, E and F) and 293 cells (see Figs. 5B and 6B, control cells). As shown by the asterisks in Fig. 2, these vacuoles often had multi-lamellar structures, which are characteristic of late endocytic vesicles (late endosome and lysosome).

Rheb Localizes to Endocytic Rab7- and Rab9-Positive Vesicles—To identify the nature of the large vacuoles in which Rheb localized, some members of the Rab GTPase family tagged with Dsred were simultaneously expressed in MDCK cells as organelle markers specific for each subcellular compartment. As shown in Fig. 3, A and D, Rab5 and Rab11, which are involved in early endosome formation and endosomal recycling, respectively, showed distinct staining patterns from Rheb. On the other hand, Rab7 and Rab9, used as late endocytic markers, mostly co-localized with Rheb in the enlarged vacuoles (Fig. 3, B and C). These data correlate with the observation that Rheb localizes in the multi-lamellar late endocytic vesicles. When the amount of Rheb transfected was increased, we observed partial co-localization of Rab5 in the Rheb-induced vacuoles (data not shown), suggesting that hybrids of early and late endocytic organelles were created.

Vacuole Formation Is Affected by the GTPase Cycle of Rheb—Rheb has been characterized as a unique small GTPase in which critical amino acids necessary for

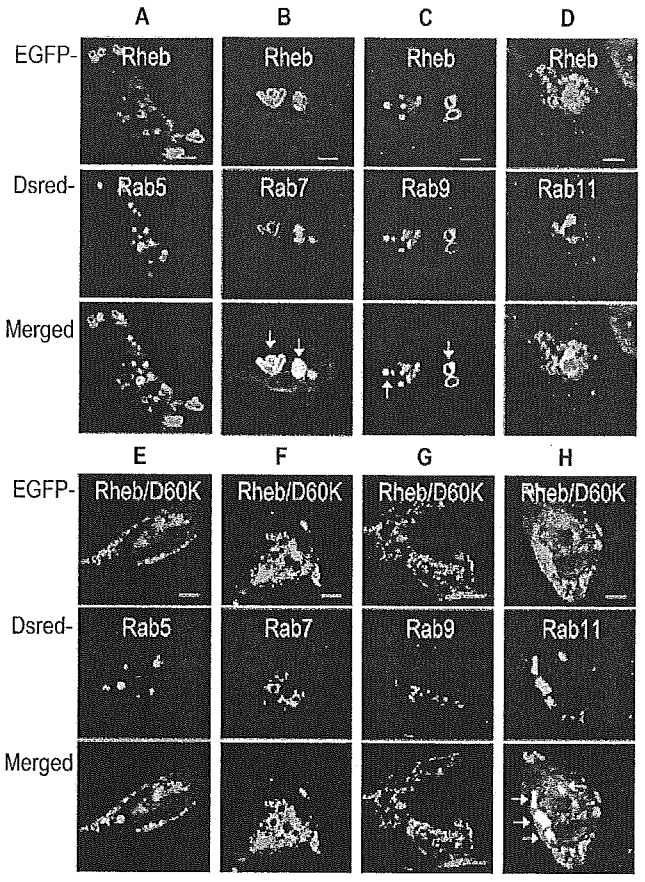

Fig. 3. **Rheb co-localizes with Rab7 and Rab9 in multi-vesicular structures, whereas Rheb/D60K mutant co-localizes partly with Rab11-containing vesicles.** MDCK cells were transfected with EGFP-Rheb (A–D) or EGFP-Rheb/D60K (E–H), together with Dsred-Rab5 (A and E), Dsred-Rab7 (B and F), Dsred-Rab9 (C and G) or Dsred-Rab11 (D and H), and further incubated for 16 h. The fluorescence of EGFP (upper) and Dsred (middle) was visualized by the confocal microscopy. Merged images of the two signals are also illustrated (bottom). Scale bars indicate 5 μm.

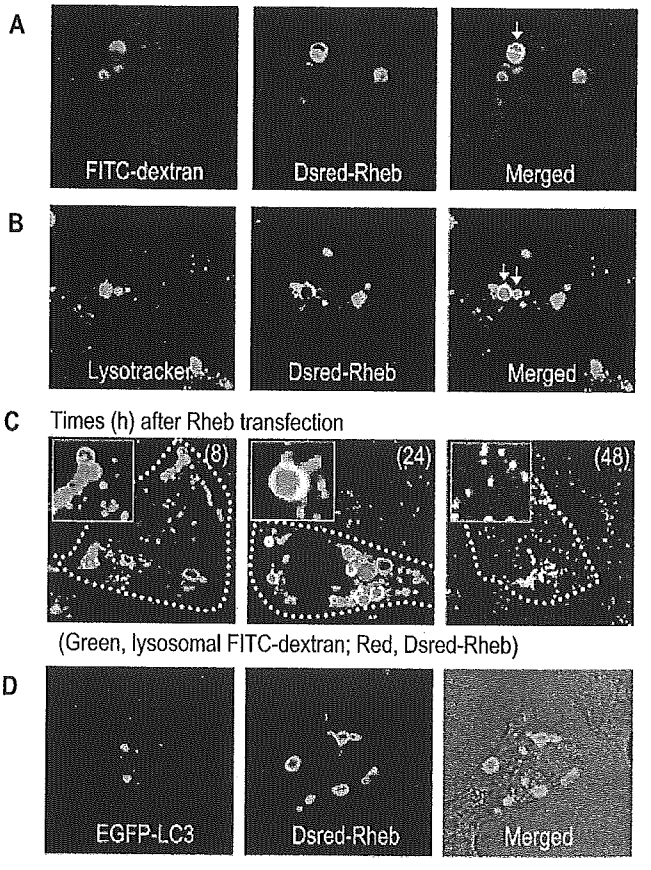

Fig. 4. **Rheb-positive vesicles are translocated from late endosomes to lysosomes.** A and B, MDCK cells transfected with Dsred-Rheb (A and B) were incubated with 1 mg/ml of FITC-dextran for 12 h (A) or 50 nM Lysotracker Green for 1 h (B). C, MDCK cells, of which lysosomal fractions had been labeled with FITC-dextran, were transfected with Dsred-Rheb and further incubated for the indicated times. The left upper insets show the enlargement of a part of the images, and the white dotted line indicates a single Rheb-transfected cell. D, MDCK cells were transfected with EGFP-LC3 and Dsred-Rheb and cultured for 16 h. The fluorescent and merged images are illustrated.

GTPase reaction are not conserved (*3*). This implies that Rheb may exist in living cells mostly as a GTP-bound form (*1*). Furthermore, a mutant Rheb, Rheb/D60K, has recently been reported to exhibit a dominant-negative effect on the activation of the mTOR pathway (*24*). To confirm the nucleotide-bound status of the wild-type and mutant Rhebs, HeLa cells were transfected with the FLAG-tagged proteins and cultured in $^{32}P_i$-containing medium. The recombinant proteins were immunoprecipitated, and the radiolabeled nucleotides associating with the proteins were analyzed by thin-layer chromatography. As expected, wild-type Rheb and Rheb/D60K existed mostly as GTP-bound and GDP-bound forms, respectively (data not shown).

We next examined how the nucleotide-bound forms of Rheb are localized in MDCK cells. In contrast to wild-type Rheb (see Fig. 2A), the expression of Rheb/D60K did not induce large vacuoles, but the mutant protein localized in intracellular small vesicles (Fig. 2D). As shown in Fig. 3, F and G, co-staining with Rab7 and Rab9 revealed that Rheb/D60K localized was quite differently from the wild-type protein, but abutting on late endocytic vesicles (compare with B and C). Rab5 also did not co-localize with the Rheb/D60K signals (E). However, recycling endosomes associating with Rab11 showed partial co-localization with Rheb/D60K (H). It should be noted here that the vesicular localization of each Rab protein was not markedly affected by the transfection of the wild-type or the mutant Rheb proteins (compare panels A–D with E–H). These data suggest that the subcellular localization of Rheb changed depending on its nucleotide-bound state.

Rheb-Positive Vesicles Are Translocated from Late Endosomes to Lysosomes—We further investigated how the Rheb-positive vesicles are created in the membrane trafficking pathway by comparing the localization of various endocytic makers. As shown in Fig. 4A, FITC-dextran, which is a non-selective endocytic marker that is able to reach late endosomes and lysosomes, was found to be present partly in lumens of the Rheb-positive vesicles. Lysotracker, a labeling probe for acidic organelles such as lysosomes (*25*), also accumulated in the Rheb-positive structures (Fig. 4B), indicating that parts of the Rheb-positive vesicles had acidic characteristics. We also investigated the time-dependent formation of Rheb-positive vesicles in MDCK cells, of which the lysosomal fraction had been selectively labeled with FITC-dextran. As shown in Fig. 4C, Rheb-positive vesicles were evident at 8 h after the transfection, but their distribution never co-localized with FITC-dextran, indicating that the early stage of expressed Rheb is not present in lysosomes. However, some Rheb signals co-localized with the FITC-dextran at 24 h, and most of the Rheb signals moved to the FITC-labeled lysosome at 48 h, suggesting that Rheb vesicles are gradually translocated to lysosomal compartments. These results are consistent with the previous results showing the co-localization of Rheb with Rab7 and Rab9 (see Fig. 3, B and C). Thus, the Rheb-positive vesicles appeared to be created at least from endocytic (or unidentified) organelles and gradually to fuse with lysosomes through late endosomes.

To further confirm the late endocytic localization of Rheb signals, we attempted to immunostain the Rheb-transfected cells with antibodies specific for late endocytic organelles. However, the Rheb-containing vesicles were fragmented during the process of fixation, and the localization of Rheb in the fixed cells appeared to be different from that in the living cells (data not shown). We could not overcome this problem with any of several fixation methods tested. Nevertheless, we would like to propose that the Rheb-induced vesicles have characteristics of late endocytic organelles based on the following observations. First, Rheb could co-localize with Rab7 and Rab9 but not with Rab5 or Rab11. Second, Rheb-induced organelles contained the endocytic marker FITC-dextran. Third, Rheb-induced vesicles were characterized as acidic organelles. Fourth, Rheb-containing vesicles gradually became positive for lysosomal markers.

The Rheb-positive vesicles seemed to share similar characteristics with autophagosomes in terms of Rab7-positive, lysosome-fusible, and multi-lamellar structures (*26, 27*). Moreover, mTOR, which is a downstream kinase of Rheb GTPase, appears to function as a negative regulator of autophagy (*17, 28*). Therefore, we analyzed whether Rheb signals co-localize with the autophagosome marker LC3, since Rheb-positive structures might be parts of accumulated incomplete autophagosomes due to the inhibition of autophagy through the activation of mTOR kinase. However, EGFP-LC3 signals never co-localized with Dsred-Rheb (Fig. 4D). When the transfected cells were starved by serum depletion, there was a marked elevation of the LC3 signals lacking co-localization with Rheb (data not shown). These data suggest that Rheb-positive vesicles are different entities from autophagosomes.

PI3k-Akt Signaling May Be Involved in the Upstream Pathway of the Rheb-Induced Vacuole Formation—As mentioned before, PI3k-Akt signaling appears to be involved in the upstream pathway of Rheb activation. To investigate whether inhibition of PI3k affects the Rheb-induced vacuole formation, the transfected 293 cells were incubated with the specific inhibitor LY294002, under which conditions PI3k activity was entirely suppressed. The effectiveness of the sustained PI3k inhibition was confirmed by measuring the phosphorylation of GSK-3β, a direct substrate of Akt. As shown in Fig. 5A, the inhibition of PI3k was clearly evident even after incubation of the cells with LY294002 for 16 h. Under these conditions, Rheb-induced large vacuole formation was markedly impaired in 293 cells (Fig. 5B). Instead, small punctated Rheb-positive vesicles were evident in the LY294002-treated cells, which are reminiscent of Rheb/D60K-induced vesicles (see Fig. 2D). This suggests that LY294002 probably activates endogenous GAP, so that expressed Rheb is rapidly deactivated and fails to induce large vacuoles under these conditions. These results may indicate that PI3k-Akt signaling is situated in the upstream of the pathway involved in the large vacuole formation. However, the PI3k activity has been also known to regulate various aspects of endosomal and lysosomal functions and membrane trafficking independent of Rheb functions (*29*). Thus, the GAP-sensitive GTPase cycle of Rheb appears to partly regulate the endocytic pathway from late endosomes to lysosomes, although we can not totally rule out the possibility that impaired vacuole formation in LY294002-treated cells is due to the inhibition of other

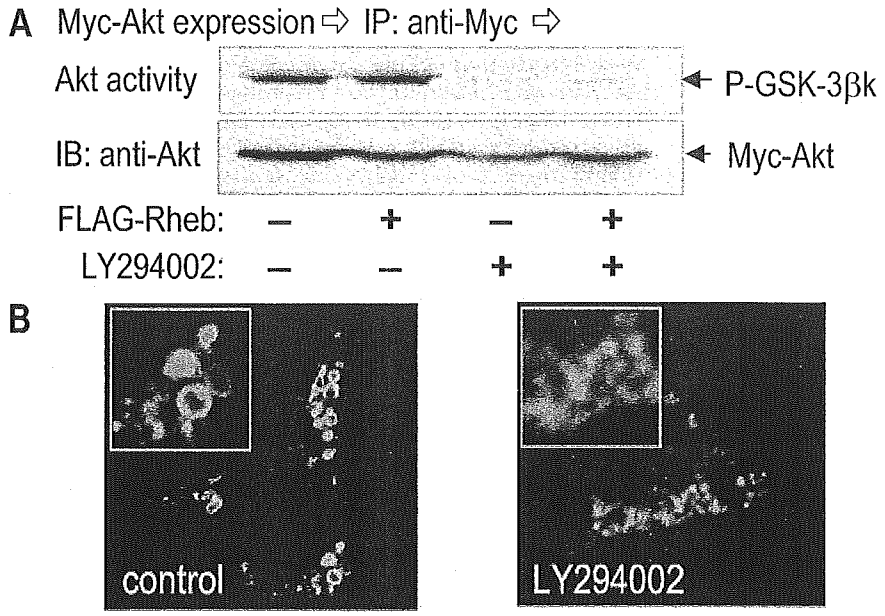

Fig. 5. **PI3k-Akt signaling may be involved in the Rheb-induced vacuole formation.** 293 cells that had been transfected with Myc-Akt and FLAG-Rheb (A) or Dsred-Rheb (B) were incubated in the presence or absence of 50 μM LY294002. A, the cell lysates were prepared and subjected to immunoprecipitation (IP) with an anti-Myc antibody, and the kinase activity and protein amount of Akt in the precipitated fractions were measured as described under "MATERIALS AND METHODS." B, the fluorescence of Dsred was visualized by confocal microscopy. The left upper insets show the enlargement of a part of the images.

endosomal target(s), which is regulated by the activity of PI3k.

Rheb-Induced Vacuolar Formation Is Independent of the Activation of mTOR—It has been reported that Rheb stimulates the kinase activity of mTOR, which leads to the activation of S6K responsible for protein synthesis (*16*). To investigate whether the activation of mTOR kinase is necessary for the induction of Rheb-positive vacuoles, 293 cells were transfected with FLAG-Rheb under conditions whereby mTOR activity was entirely suppressed with the specific inhibitor rapamycin. The effectiveness of the mTOR inhibition was confirmed by measuring the phosphorylation of p70 S6K, a direct substrate of mTOR. As shown in Fig. 6A, the inhibition of mTOR was clearly observed even after prolonged incubation of the cells with rapamycin. However, there was no marked difference in the Rheb-positive vacuole formation between the control and rapamycin-treated cells (Fig. 6B). These data indicate that the activation of mTOR is not required for the Rheb-induced vacuole formation.

The Possible Role of Rheb-Induced Vacuole Formation in Cell Functions Other than Cell Growth and Cell-Cycle Progression—The present study has revealed that Rheb activation induces large vacuoles in cytoplasm of the

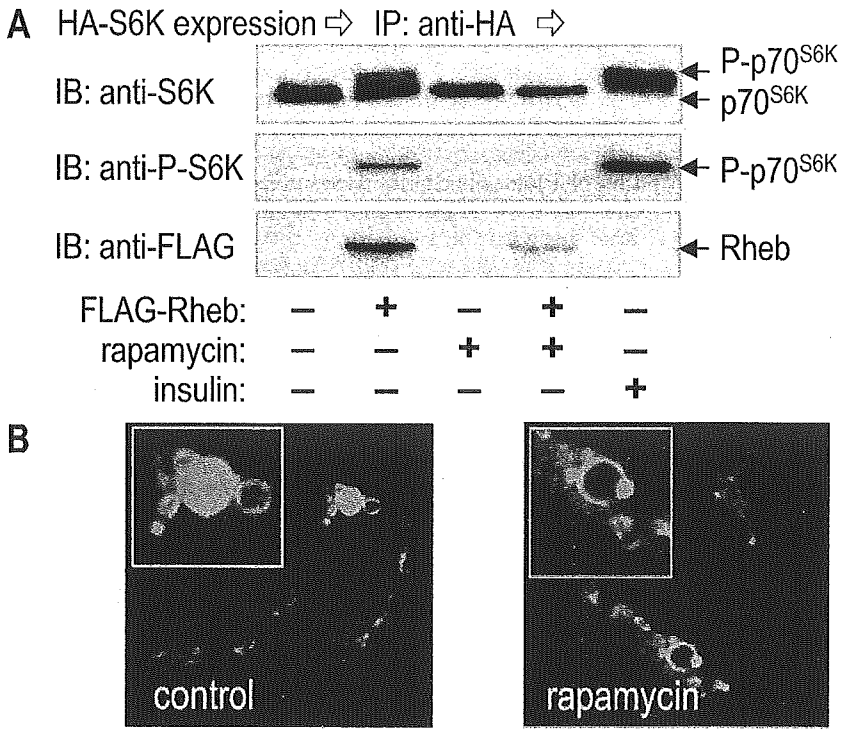

Fig. 6. **Activation of mTOR kinase is not required for the Rheb-induced vacuole formation.** 293 cells that had been transfected with FLAG-Rheb and HA-p70 S6K (A) or Dsred-Rheb (B) were incubated in the presence or absence of 40 nM rapamycin. A, as a control, the transfected HA-p70 S6 kinase was stimulated by incubation of cells with 200 nM insulin. Cell lysates were prepared and immunoprecipitated with an anti-HA antibody. The precipitated fractions were separated by SDS-PAGE and subjected to immunoblot analysis with anti–p70 S6K (upper) or anti–phosphorylated p70 S6K (middle) antibodies. The cell lysates were also immunoblotted with an anti-FLAG antibody (bottom). B, the fluorescence of Dsred was visualized by confocal microscopy. The left upper insets show the enlargement of a part of the images.

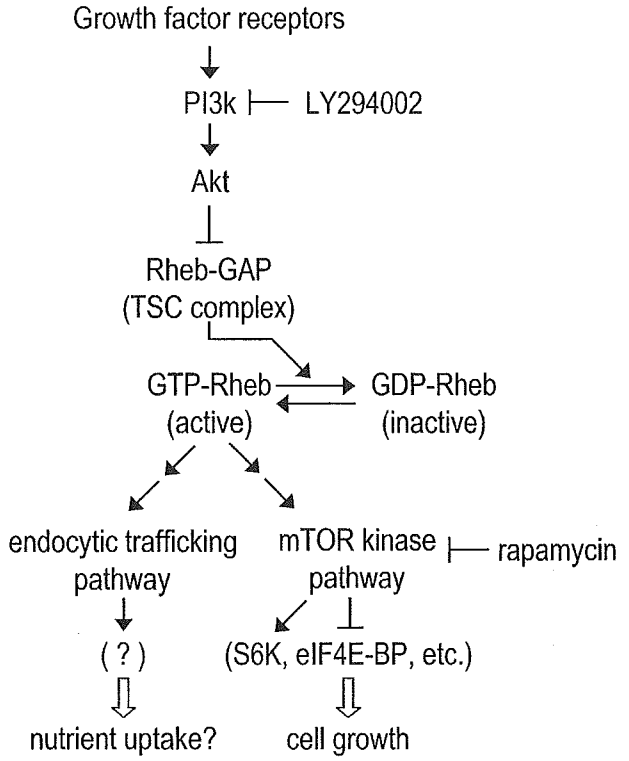

Fig. 7. **Schematic representation of Rheb-related signal transduction pathways.** Rheb induces not only the activation of mTOR kinase leading to cell growth but also late-endocytic vesicle formation that may play a critical role in nutrient uptake. See text for further explanation.

transfected cells and that the vacuoles are characterized as late endosome- or lysosome-like organelles. Moreover, the large vacuole formation is dependent on the GTPase cycle of Rheb and probably the stimulation of the PI3k-Akt pathway, but not on the activation of mTOR kinase. These data suggest that Rheb-induced vacuole formation is a novel Rheb-downstream pathway that is distinguishable from the activation of mTOR kinase pathway (Fig. 7). Rheb was first identified as a gene whose mRNA expression is increased in rat brain by seizures or by the stimulation of long-term potentiation (*3*). Since then, several groups has examined whether Rheb is involved in the activation of Raf, the well-known downstream kinase of conventional Ras (*30–33*). The recent identification of Rheb as a positive regulator of mTOR pathway has attracted considerable attention, in addition to the report that TSC acts as a GAP for Rheb (*1*, *15*, *34*, *35*). To our knowledge, however, this is the first report that indicates the involvement of Rheb in the endocytic pathway.

In yeast, several reports suggest that TSC positively and Rheb negatively regulate arginine uptake (*18–20*). In addition, Tsc1 and Tsc2 knockouts in *S. pombe* exhibited abnormal intracellular distribution of an amino-acid permease (*21*). It is, therefore, tempting to speculate that the activation of Rheb induces endocytic vacuoles that may have an effect on the localization of permeases. Our preliminary experiments indicate that Rheb is capable of interacting directly with several channels or transporters implicated in nutrient uptake. Moreover, these transporters were selectively translocated from the plasma membrane to Rheb-induced vacuoles in Rheb-transfected cells. These results suggest that Rheb-induced vacuoles are necessary for nutrient regulation through their translocation (Fig. 7). Further investigation is needed to uncover the physiological roles of Rheb, and it is important to investigate the regulation of the endocytic pathway in terms of nutrient uptake, in which Rheb-pathway may play a critical role.

This work was supported in part by research grants from the Ministry of Education, Culture, Sports, Science and Technology (MEXT) of the Japanese Government, the Japan Society for the Promotion of Science (JSPS), the Mitsubishi Foundation, and the Uehara Memorial Foundation.

REFERENCES

1. Li, Y., Corradetti, M.N., Inoki, K., and Guan, K.L. (2004) TSC2: filling the GAP in the mTOR signaling pathway. *Trends Biochem. Sci.* **29**, 32–38
2. Kontani, K., Tada, M., Ogawa, T., Okai, T., Saito, K., Araki, Y., and Katada, T. (2002) Di-Ras, a distinct subgroup of ras family GTPases with unique biochemical properties. *J. Biol. Chem.* **277**, 41070–41078
3. Yamagata, K., Sanders, L.K., Kaufmann, W.E., Yee, W., Barnes, C.A., Nathans, D., and Worley, P.F. (1994) rheb, a growth factor- and synaptic activity-regulated gene, encodes a novel Ras-related protein. *J. Biol. Chem.* **269**, 16333–16339
4. Patel, P.H., Thapar, N., Guo, L., Martinez, M., Maris, J., Gau, C.L., Lengyel, J.A., and Tamanoi, F. (2003) *Drosophila* Rheb GTPase is required for cell cycle progression and cell growth. *J. Cell Sci.* **116**, 3601–3610
5. Inoki, K., Li, Y., Xu, T., and Guan, K.L. (2003) Rheb GTPase is a direct target of TSC2 GAP activity and regulates mTOR signaling. *Gene. Dev.* **17**, 1829–1834
6. Garami, A., Zwartkruis, F.J., Nobukuni, T., Joaquin, M., Roccio, M., Stocker, H., Kozma, S.C., Hafen, E., Bos, J.L., and Thomas, G. (2003) Insulin activation of Rheb, a mediator of mTOR/S6K/4E-BP signaling, is inhibited by TSC1 and 2. *Mol. Cell* **11**, 1457–1466
7. Castro, A.F., Rebhun, J.F., Clark, G.J., and Quilliam, L.A. (2003) Rheb binds tuberous sclerosis complex 2 (TSC2) and promotes S6 kinase activation in a rapamycin- and farnesylation-dependent manner. *J. Biol. Chem.* **278**, 32493–32496
8. Tee, A.R., Manning, B.D., Roux, P.P., Cantley, L.C., and Blenis, J. (2003) Tuberous sclerosis complex gene products, Tuberin and Hamartin, control mTOR signaling by acting as a GTPase-activating protein complex toward Rheb. *Curr. Biol.* **13**, 1259–1268
9. Saucedo, L.J., Gao, X., Chiarelli, D.A., Li, L., Pan, D., and Edgar, B.A. (2003) Rheb promotes cell growth as a component of the insulin/TOR signalling network. *Nat. Cell Biol.* **5**, 566–571
10. Stocker, H., Radimerski, T., Schindelholz, B., Wittwer, F., Belawat, P., Daram, P., Breuer, S., Thomas, G., and Hafen, E. (2003) Rheb is an essential regulator of S6K in controlling cell growth in *Drosophila*. *Nat. Cell Biol.* **5**, 559–565
11. Zhang, Y., Gao, X., Saucedo, L.J., Ru, B., Edgar, B.A., and Pan, D. (2003) Rheb is a direct target of the tuberous sclerosis tumour suppressor proteins. *Nat. Cell Biol.* **5**, 578–581
12. Franke, T.F., Yang, S.I., Chan, T.O., Datta, K., Kazlauskas, A., Morrison, D.K., Kaplan, D.R., and Tsichlis, P.N. (1995) The protein kinase encoded by the Akt proto-oncogene is a target of the PDGF-activated phosphatidylinositol 3-kinase. *Cell* **81**, 727–736
13. Burgering, B.M. and Coffer, P.J. (1995) Protein kinase B (c-Akt) in phosphatidylinositol-3-OH kinase signal transduction. *Nature* **376**, 599–602

14. Inoki, K., Li, Y., Zhu, T., Wu, J., and Guan, K.L. (2002) TSC2 is phosphorylated and inhibited by Akt and suppresses mTOR signalling. *Nat. Cell Biol.* **4**, 648–657
15. Manning, B.D. and Cantley, L.C. (2003) Rheb fills a GAP between TSC and TOR. *Trends Biochem. Sci.* **28**, 573–576
16. Fingar, D.C. and Blenis, J. (2004) Target of rapamycin (TOR): an integrator of nutrient and growth factor signals and coordinator of cell growth and cell cycle progression. *Oncogene* **23**, 3151–3171
17. Raught, B., Gingras, A.C., and Sonenberg, N. (2001) The target of rapamycin (TOR) proteins. *Proc. Natl Acad. Sci. USA* **98**, 7037–7044
18. van Slegtenhorst, M., Carr, E., Stoyanova, R., Kruger, W.D., and Henske, E.P. (2004) Tsc1+ and tsc2+ regulate arginine uptake and metabolism in *Schizosaccharomyces pombe*. *J. Biol. Chem.* **279**, 12706–12713
19. Urano, J., Tabancay, A.P., Yang, W., and Tamanoi, F. (2000) The *Saccharomyces cerevisiae* Rheb G-protein is involved in regulating canavanine resistance and arginine uptake. *J. Biol. Chem.* **275**, 11198–11206
20. Mach, K.E., Furge, K.A., and Albright, C.F. (2000) Loss of Rhb1, a Rheb-related GTPase in fission yeast, causes growth arrest with a terminal phenotype similar to that caused by nitrogen starvation. *Genetics* **155**, 611–622
21. Matsumoto, S., Bandyopadhyay, A., Kwiatkowski, D.J., Maitra, U., and Matsumoto, T. (2002) Role of the Tsc1-Tsc2 complex in signaling and transport across the cell membrane in the fission yeast *Schizosaccharomyces pombe*. *Genetics* **161**, 1053–1063
22. Saito, K., Murai, J., Kajiho, H., Kontani, K., Kurosu, H., and Katada, T. (2002) A novel binding protein composed of homophilic tetramer exhibits unique properties for the small GTPase Rab5. *J. Biol. Chem.* **277**, 3412–3418
23. Kajiho, H., Saito, K., Tsujita, K., Kontani, K., Araki, Y., Kurosu, H., and Katada, T. (2003) RIN3: a novel Rab5 GEF interacting with amphiphysin II involved in the early endocytic pathway. *J. Cell Sci.* **116**, 4159–4168
24. Tabancay, A.P., Jr., Gau, C.L., Machado, I.M., Uhlmann, E.J., Gutmann, D.H., Guo, L., and Tamanoi, F. (2003) Identification of dominant negative mutants of Rheb GTPase and their use to implicate the involvement of human Rheb in the activation of p70S6K. *J. Biol. Chem.* **278**, 39921–39930
25. Bucci, C., Thomsen, P., Nicoziani, P., McCarthy, J., and van Deurs, B. (2000) Rab7: a key to lysosome biogenesis. *Mol. Biol. Cell* **11**, 467–480
26. Gutierrez, M., Munafo, D., Beron, W., and Colombo, M. (2004) Rab7 is required for the normal progression of the autophagic pathway in mammalian cells. *J. Cell Sci.* **117**, 2687–2697
27. Gozuacik, D. and Kimchi, A. (2004) Autophagy as a cell death and tumor suppressor mechanism. *Oncogene* **23**, 2891–2906
28. Kamada, Y., Sekito, T., and Ohsumi, Y. (2004) Autophagy in yeast: a TOR-mediated response to nutrient starvation. *Curr. Top. Microbiol. Immunol.* **279**, 73–84
29. Simonsen, A., Wurmser, A.E., Emr, S.D., and Stenmark, H. (2001) The role of phosphoinositides in membrane transport. *Curr. Opin. Cell Biol.* **13**, 485–492
30. Clark, G.J., Kinch, M.S., Rogers-Graham, K., Sebti, S.M., Hamilton, A.D., and Der, C.J. (1997) The Ras-related protein Rheb is farnesylated and antagonizes Ras signaling and transformation. *J. Biol. Chem.* **272**, 10608–10615
31. Yee, W.M. and Worley, P.F. (1997) Rheb interacts with Raf-1 kinase and may function to integrate growth factor- and protein kinase A-dependent signals. *Mol. Cell. Biol.* **17**, 921–933
32. Im, E., von Lintig, F.C., Chen, J., Zhuang, S., Qui, W., Chowdhury, S., Worley, P.F., Boss, G.R., and Pilz, R.B. (2002) Rheb is in a high activation state and inhibits B-Raf kinase in mammalian cells. *Oncogene* **21**, 6356–6365s
33. Karbowniczek, M., Cash, T., Cheung, M., Robertson, G.P., Astrinidis, A., and Henske, E.P. (2004) Regulation of B-Raf kinase activity by tuberin and Rheb is mammalian target of rapamycin (mTOR)-independent. *J. Biol. Chem.* **279**, 29930–29937
34. Pan, D., Dong, J., Zhang, Y., and Gao, X. (2004) Tuberous sclerosis complex: from *Drosophila* to human disease. *Trends Cell Biol.* **14**, 78–85
35. Aspuria, P. and Tamanoi, F. (2004) The Rheb family of GTP-binding proteins. *Cell Signal.* **16**, 1105–1112

Cell Tissue Res
DOI 10.1007/s00441-005-0077-0

REGULAR ARTICLE

Tsuyoshi Ishikawa · Shuji Terai · Yohei Urata · Yoshio Marumoto · Koji Aoyama · Isao Sakaida · Tomoaki Murata · Hiroshi Nishina · Koh Shinoda · Shunji Uchimura · Yoshihiko Hamamoto · Kiwamu Okita

Fibroblast growth factor 2 facilitates the differentiation of transplanted bone marrow cells into hepatocytes

Received: 25 May 2005 / Accepted: 9 August 2005
© Springer-Verlag 2005

Abstract We have developed an in vivo mouse model, the green fluorescent protein (GFP)/carbon tetrachloride (CCl_4) model, and have previously reported that transplanted GFP-positive bone marrow cells (BMCs) differentiate into hepatocytes via hepatoblast intermediates. Here, we have investigated the growth factors that are closely related to the differentiation of transplanted BMCs into hepatocytes, and the way that a specific growth factor affects the differentiation process in the GFP/CCl_4 model. We performed immunohistochemical analysis to identify an important growth factor in our model, viz., fibroblast growth factor (FGF). In liver samples, the expression of FGF1 and FGF2 and of FGF receptors (FGFRs; FGFR1, FGFR2) was significantly elevated with time after bone marrow transplantation (BMT) compared with other factors, and co-expression of GFP and FGFs or FGFRs could be detected. We then analyzed the effect and molecular mechanism of FGF signaling on the enhancement of BMC differentiation into hepatocytes by immunohistochemistry, immunoblotting, and microarray analysis. Treatment with recombinant FGF (rFGF), especially rFGF2, elevated the repopulation rate of GFP-positive cells in the liver and significantly increased the expression of both Liv2 (hepatoblast marker) and albumin (hepatocyte marker). Administration of rFGF2 at BMT also raised serum albumin levels and improved the survival rate. Transplantation of BMCs with rFGF2 specifically activated tumor necrosis factor-alpha (TNF-α) signaling. Thus, FGF2 facilitates the differentiation of transplanted BMCs into albumin-producing hepatocytes via Liv2-positive hepatoblast intermediates through the activation of TNF-α signaling. Administration of FGF2 in combination with BMT improves the liver function and prognosis of mice with CCl_4-induced liver damage.

Keywords Bone marrow cell · Stem cell · Hepatocyte · Differentiation · Liver · Fibroblast growth factor · Tumor necrosis factor · Mouse

Abbreviations BMC: bone marrow cell · BMT: bone marrow transplantation · GFP: green fluorescent protein · CCl_4: carbon tetrachloride · SOM: self-organizing map · FGF: fibroblast growth factor · EGF: epidermal growth factor · EGFR: epidermal growth factor receptor · FGFR: fibroblast growth factor receptor · HGF: hepatocyte growth factor · VEGF: vascular endothelial growth factor · VEGFR: vascular endothelial growth factor receptor ·

This study was supported by Grants-in-Aid for Scientific Research from the Japan Society for the Promotion of Science (nos. 13470121, 13770262, 15790348, 16390211, and 16590597) and for translational research from the Ministry of Health, Labor and Welfare (H-trans-5).

T. Ishikawa · S. Terai (✉) · Y. Urata · Y. Marumoto · K. Aoyama · I. Sakaida · K. Okita
Department of Molecular Science & Applied Medicine (Gastroenterology & Hepatology),
Yamaguchi University School of Medicine,
Minami Kogushi 1-1-1, Ube,
755-8505 Yamaguchi, Japan
e-mail: terais@yamaguchi-u.ac.jp
Tel.: +81-836-222241
Fax: +81-836-222240

T. Murata
Science Research Center, Yamaguchi University,
Minami Kogushi 1-1-1, Ube,
755-8505 Yamaguchi, Japan

H. Nishina
Department of Developmental and Regenerative Biology,
Medical Research Institute,
Tokyo Medical and Dental University,
1-5-45, Yushima, Bunkyo-ku,
Tokyo, 113-8510, Japan

K. Shinoda
Department of Neuroanatomy & Neuroscience,
Yamaguchi University School of Medicine,
Minami Kogushi 1-1-1, Ube,
755-8505 Yamaguchi, Japan

S. Uchimura · Y. Hamamoto
Department of Computer Science and Systems Engineering,
Faculty of Engineering, Yamaguchi University,
Tokiwadai 2-16-1, Ube,
755-8611 Yamaguchi, Japan

PDGF: platelet-derived growth factor · PDGFR: platelet-derived growth factor receptor · TGFβ: transforming growth factor β · TGFβR: transforming growth factor β receptor · rFGF: recombinant fibroblast growth factor · TNF-α: tumor necrosis factor-α · TNFIP3: tumor necrosis factor-α induced protein 3 · NF-κB: nuclear factor-κB

Introduction

Liver cirrhosis is the end-stage of chronic liver disease and is extremely difficult to treat. Currently, liver transplantation is one of the effective therapies available to patients who face this life-threatening condition. However, this treatment presents serious problems, such as the lack of a donor, operative damage, rejection, and high cost. Regenerative therapy by stem cell transplantation is a promising approach for the treatment of patients with severe liver disease. The capacity of bone marrow cells (BMCs) to differentiate into hepatocytes and intestinal cells was first identified through the detection of Y-chromosome-containing cells in postmortem samples from female recipients of BMCs from male donors (Alison et al. 2000; Theise et al. 2000). Bone marrow transplantation (BMT) is now an established treatment for hematological diseases, and several clinical studies have evaluated the potential of BMCs in regeneration of the myocardium and blood vessels (Orlic et al. 2001; Stamm et al. 2003; Wexler et al. 2003). Together, these findings suggest that BMCs will be an effective cell source for regenerative therapy in the liver.

To realize the potential for cell therapy by BMCs, we have developed an in vivo mouse model to monitor the differentiation of BMCs into hepatocytes, viz., the green fluorescent protein (GFP)/carbon tetrachloride (CCl_4) model (Terai et al. 2003). We have shown that transplanted GFP-positive BMCs populate the damaged liver and differentiate into albumin-producing hepatocytes via hepatoblast intermediates under CCl_4-induced persistent liver-damage conditions (Terai et al. 2003; Yamamoto et al. 2004). Furthermore, BMT elevates serum albumin levels, reduces liver fibrosis, and improves the survival rate of CCl_4-treated mice (Sakaida et al. 2004). These results suggest that BMT could become an effective treatment for patients with liver failure.

Several lines of evidence support the idea that chronic liver injury by CCl_4 is required to induce the differentiation of transplanted stem cells into hepatocyte-like cells (Wang et al. 2003; Kollet et al. 2003). In our model, similarly, some feature associated with continuous intraperitoneal administration of CCl_4, which causes persistent liver damage, actually appears to facilitate or induce migration of BMCs to the liver and differentiation of BMCs into hepatocytes. In addition, we have used microarray analysis, together with a self-organizing map (SOM), to show that dramatic gene activation occurs after BMT into mice with CCl_4-induced liver damage (Omori et al. 2004). Genes associated with morphology are activated at an early stage, whereas genes that regulate differentiation of hepatocytes are up-regulated at a later stage.

Growth factors are known to affect cell proliferation and differentiation and reportedly participate in repair processes of many organs. Moreover, clinical trials have been carried out with several growth factors for the therapy of peripheral vascular disorders, ischemic heart diseases, and cutaneous chronic wounds through neoangiogenesis (Laham et al. 2000; Lederman et al. 2002; Fu et al. 2002). Here, we report the identification of a growth factor that induces cellular repopulation of damaged liver and the differentiation of transplanted BMCs into hepatocytes. Furthermore, we report the results of our investigation into the way that the identified growth factor, namely fibroblast growth factor (FGF), affects these processes in the GFP/CCl_4 mouse model of liver damage and regenerative treatment.

Materials and methods

Experimental protocol: GFP/CCl_4 model

C57 BL/6 Tg14 (act-EGFP) OsbY01 mice (GFP transgenic mice) were kindly provided by Dr. Masaru Okabe (Genome Research Center, Osaka University, Osaka, Japan), and C57 BL/6 female mice were purchased from Japan SLC (Shizuoka, Japan). In this study, injection of 1.0 ml/kg body weight of CCl_4 into recipient mice was performed at 6 weeks of age via the peritoneum twice a week for 4 weeks to induce persistent liver damage. On one day after 4 weeks of CCl_4 treatment, 1×10^5 GFP-positive BMCs were transplanted slowly, by using a 31-gauge needle and Hamilton syringe, via the tail vein as previously described (Terai et al. 2003). After BMT, the same dose of CCl_4 was continuously injected twice a week to maintain persistent liver damage. Mice treated with CCl_4 without BMT were used as a control group. Individual mice were killed at 48 h and every week after BMT. All processes, including surgical steps, conformed to the guidelines of Yamaguchi University for animal and recombinant DNA experiments.

Immunohistochemical staining

We obtained liver samples from six independent mice in each group, and immunohistochemical staining was performed as previously described (Shinoda et al. 1992). Immunohistochemical samples were quantified by using a Provis microscope (Olympus, Tokyo, Japan) equipped with a charge-coupled device camera; the obtained images were subjected to computer-assisted analysis with MetaMorph software (Universal Imaging, Downingtown, Pa.). A total of 30 random fields per group were analyzed independently, and the percentage of stained area was calculated by using MetaMorph software. For screening, we examined the expression of several growth factor receptors by using commercial antibodies against the following: epidermal growth factor (EGF) receptor (EGFR), FGF receptor 1 (FGFR1), and FGFR2, all from Santa Cruz Biotechnology (Calif., USA); hepatocyte growth factor (HGF) receptor (c-Met) from R&D Systems (Minn., USA); vascular

endothelial growth factor (VEGF) receptor 1 (VEGFR1), VEGFR2, platelet-derived growth factor (PDGF) receptor α (PDGFRα), PDGFRβ, transforming growth factor β (TGFβ) receptor 1 (TGFβR1), and TGFβR2, all from Santa Cruz Biotechnology. In addition, we analyzed the expression of FGFRs and FGFs by using antibodies against FGFR1, FGFR2, FGF1, and FGF2 (Santa Cruz Biotechnology) in two groups: the BMT(+) group that received both CCl_4 treatment and BMT, and the BMT(−) control group that received CCl_4-only treatment without BMT. Immunofluorescent detection of GFP and FGFRs or FGFs was performed with the following secondary antibodies: Alexa Fluor R-488 and R−568 donkey anti-goat IgG (H+L) conjugates and Alexa Fluor R-488 goat anti-rabbit IgG (H+L) conjugate (Molecular Probes, Eugene, Ore., USA). The analysis was performed as previously described (Terai et al. 2003; Sakaida et al. 2004).

Analysis for the effect of recombinant FGF

Recombinant FGF1 (rFGF1) or rFGF2 (R&D Systems) was administered as follows. A treatment dose of 30 μg/kg was deemed appropriate based on previous reports of clinical trials for ischemic heart diseases and peripheral vascular disorders (Laham et al. 2000; Lederman et al. 2002). C57 BL/6 female mice with CCl_4-induced chronic liver damage were divided into six groups: (1) CCl_4 group (treatment with neither BMCs nor rFGFs); (2) rFGF1 group (rFGF1-only treatment without BMT); (3) rFGF2 group (rFGF2-only treatment without BMT); (4) BMC group (BMC-only transplantation without rFGFs); (5) BMC+rFGF1 group (treatment with both BMCs and rFGF1); and (6) BMC+rFGF2 group (treatment with both BMCs and rFGF2). Isolated GFP-positive BMCs were incubated with rFGF1 or rFGF2 for approximately 30 s before transplantation and then injected into recipient mice with a 31-gauge needle and Hamilton syringe via the tail vein. After transplantation, CCl_4 injections were continued at the same dose twice a week. Mice were killed at 48 h after BMT and every week thereafter for up to 4 weeks. Immunohistochemical analysis with anti-GFP (Santa Cruz Biotechnology), anti-Liv2 (hepatoblast marker; Watanabe et al. 2002), anti-albumin (Bethyl Laboratories, Tex., USA), and anti-tumor necrosis factor-α (TNF-α; TECHNE, Min., USA) antibodies was performed on these samples (n=6 in each group). The proportion of stained area was calculated by using MetaMorph software at a total of 30 random fields per group. Moreover, serum albumin level was measured (n=6 in each group) by using the SPOTCHEM EZ SP-4430 dry chemical system (Arkray, Kyoto, Japan; Terai et al. 2003; Sakaida et al. 2004). We calculated the survival rate with follow-up for 150 days after transplantation (n=15 in each group) by using the Kaplan-Meier method.

DNA-microarray analysis: first screen and second screen

We excised an equal amount of liver sample from three independent mice in each group at 48 h and 1 week after transplantation. Total RNA was isolated from the samples by using an Atlas Glass Total RNA Isolation Kit (Clontech, Palo Alto, Calif.), and single strands of cDNA were synthesized by using an Atlas Glass Fluorescent Labeling Kit (Clontech). DNA-microarray analysis was subsequently conducted with the Atlas Glass Mouse 1.0K Microarray System (Clontech; Omori et al. 2004; Ishigaki et al. 2002). The signal intensity of each gene was measured by a fluorescent scanner (Axon Instruments, Calif., USA), and the transient differences in gene expression between two groups were assessed with the Array Gauge System (Fuji Film, Tokyo, Japan). These methods were identical to those previously performed (Omori et al. 2004). In this study, a total of 1,108 genes on the DNA-microarray were analyzed, and two screens were carried out.

We did the first screen to select genes that were significantly up-regulated by BMT with rFGF2 treatment as compared with BMT-alone. For each gene, the gene expression was analyzed by the specific equations as follows:

x_{i1}; expression level of gene i at 48 h after transplantation, in the BMC group
y_{i1}; expression level of gene i at 48 h after transplantation, in BMC+rFGF2 group
x_{i2}; expression level of gene i at 1 week after transplantation, in BMC group
y_{i2}; expression level of gene i at 1 week after the transplantation in BMC+rFGF2 group

$(i = 1, 2, 3, , , , , 1108)$

The chronological change of the expression level of gene i in each group was expressed as follows:

$$\text{BMC group; } f_{i1} = \log_{10}(x_{i2}/x_{i1})$$

$$\text{BMC + rFGF2 group; } f_{i2} = \log_{10}(y_{i2}/y_{i1})$$

The difference in the chronological change of the gene expression between two groups was defined by

$$F_i = f_{i2} - f_{i1} = \log_{10}\left[(y_{i2}/y_{i1})/(x_{i2}/x_{i1})\right]$$

If $(x_{i2}\text{-}x_{i1}) = (y_{i2}/y_{i1})$, the value of F_i, i.e., $\log_{10}1$ is zero. We focused on the genes with a large value of F.

For each gene, we computed the value of F and selected genes that fulfilled the conditions, $f_{i1}>0$, $f_{i2}>0$, and $F_i>0.477(=\log_{10}3)$. An $F_i>0.477$ means that the ratio of y_{i2}/y_{i1} to x_{i2}/x_{i1} is more than 3. These genes were considered to be significantly up-regulated by rFGF2 treatment in addition to BMT.

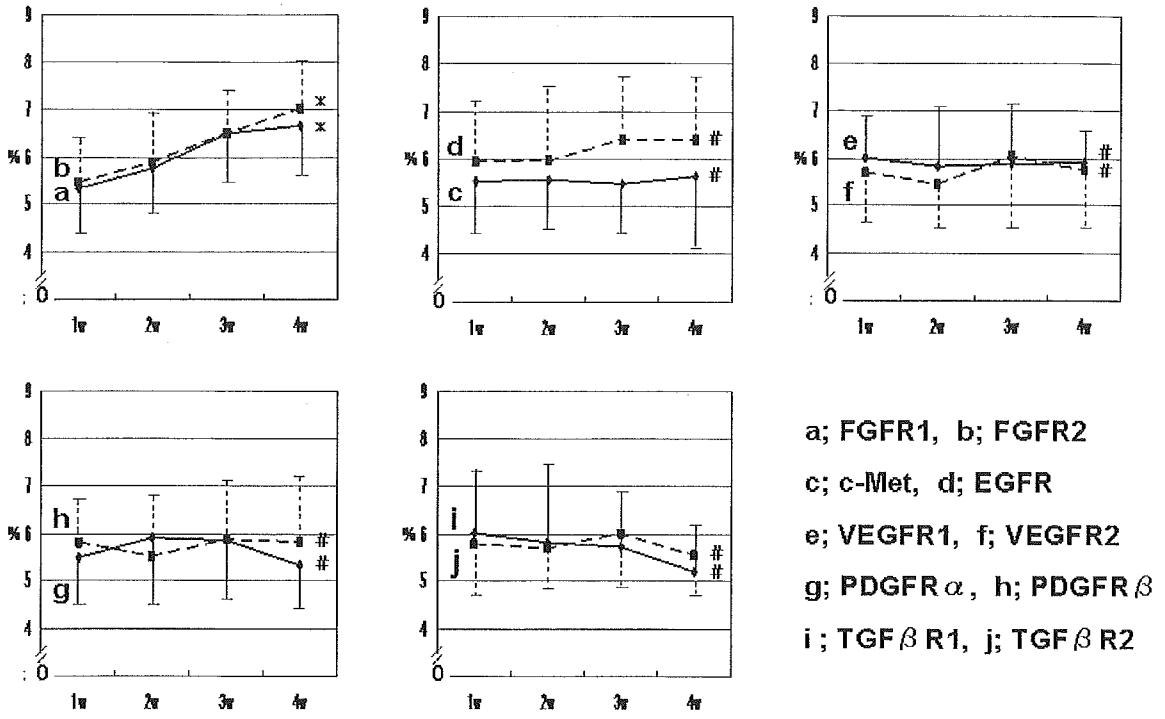

Fig. 1 Time-course of distribution of several growth factor receptors in the GFP/CCl_4 model system. Expression of FGFR1 and FGFR2 significantly increases with time after BMT (*x-axis* time after BMT (in weeks), *y-axis* percentage of stained area in immunohistochemistry). *Significant difference compared with the value at 1 week ($P<0.05$). #No significant difference compared with the value at 1 week ($P>0.05$)

We carried out the second screen to separate the gene that was most specifically activated by rFGF2 treatment with BMT out of the genes selected from the screen I. This analysis was performed by using the additional equations as follows:

$x_i'_1$; expression level of gene i at 48 h in CCl_4 group
$y_i'_1$; the expression level of gene i at 48 h in rFGF2 group
$x_i'_2$; the expression level of gene i at 1 week in CCl_4 group
$y_i'_2$; the expression level of gene i at 1 week in rFGF2 group

CCl_4 group; $f_i'_1 = \log_{10}(x_i'_2/x_i'_1)$

rFGF2 group; $f_i'_2 = \log_{10}(y_i'_2/y_i'_1)$

We compared the f value (chronological change of the gene expression) of each gene selected from screen I in two

Table 1 Percent immunohistochemically stained area in areas treated with anti-FGFR1 or anti-FGFR 2 and anti-FGF1 or anti-FGF2

Receptor or factor	Treatment	One week[a]	Four weeks[b]	Percentage change[c]
FGFR1	BMT(+)[d]	5.3%±1.0[e]	6.7%±1.1[e, f]	26.4%
	BMT(−)[g]	3.7%±0.7	4.2%±0.9	13.5%
FGFR2	BMT(+)	5.4%±0.9[e]	7.0%±1.0[e, f]	29.6%
	BMT(−)	3.8%±0.9	4.4%±1.0	15.8%
FGF1	BMT(+)	5.5%±0.9[e]	7.1%±1.0[e, f]	29.1%
	BMT(−)	3.8%±0.7	4.5%±0.5	18.4%
FGF2	BMT(+)	5.7%±1.1[e]	7.5%±1.1[e, f]	31.6%
	BMT(−)	3.9%±1.0	4.6%±1.0	17.9%

[a]One week in the BMT(−) group represents 5 weeks of CCl_4 injection
[b]Four weeks in the BMT(−) group represents 8 weeks of CCl_4 injection
[c]Percentage change over time (from 1 week to 4 weeks) in each group
[d]BMT(+): BMC transplantation group with CCl_4-induced persistent liver damage
[e]Significant difference compared with the value at same period in the BMT(−) group ($P<0.05$)
[f]Significant difference compared with the value at 1 week ($P<0.05$)
[g]BMT(−): control CCl_4-induced persistent liver damage group without BMT
BMT significantly elevates the expression of FGFRs and FGFs with time compared with the BMT (−) control group
Values are shown as means±SD

groups: the CCl_4 group and rFGF2 group. Those for the BMC group and BMC+rFGF2 group had been computed in screen I.

Western blot analysis of TNF-α

We isolated cell lysate from the liver sample at 1 week after transplantation in four groups: CCl_4 group, rFGF2 group, BMC group, and BMC+rFGF2 group. Protein was obtained by homogenization with lysis buffer (20 mM TRIS-HCl pH 7.5, 50 mM NaCl, 1 mM ethylenediaminetetraacetic acid, 1 mM ethyleneglycol-bis-N, N'-tetraacetic acid, 1% Triton X, 2.5 mM sodium pyrophosphate, 1 mM β-glycerophosphate, 1 mM Na_3VO_4, 1 μg/ml leupeptin, and 1 mM phenylmethylsulfonyl fluoride) and then centrifuged. A total of 100 μg protein were analyzed by sodium dodecylsulfate/polyacrylamide gel electrophoresis and immunoblot. Protein was electrophoretically transferred to a polyvinylidene difluoride membrane (Bio-Rad, CA, USA), which was incubated with a 1:500 dilution of goat anti-mouse TNF-α antibody, washed, and then incubated with a 1:5,000 dilution of anti-goat IgG conjugated to horseradish peroxidase (Amersham Biosciences, N.J., USA). Bands were visualized with an enhanced chemiluminescence Western blotting detection system (Amersham Biosciences, NJ, USA). All experiments were repeated independently at least three times with reproducible results.

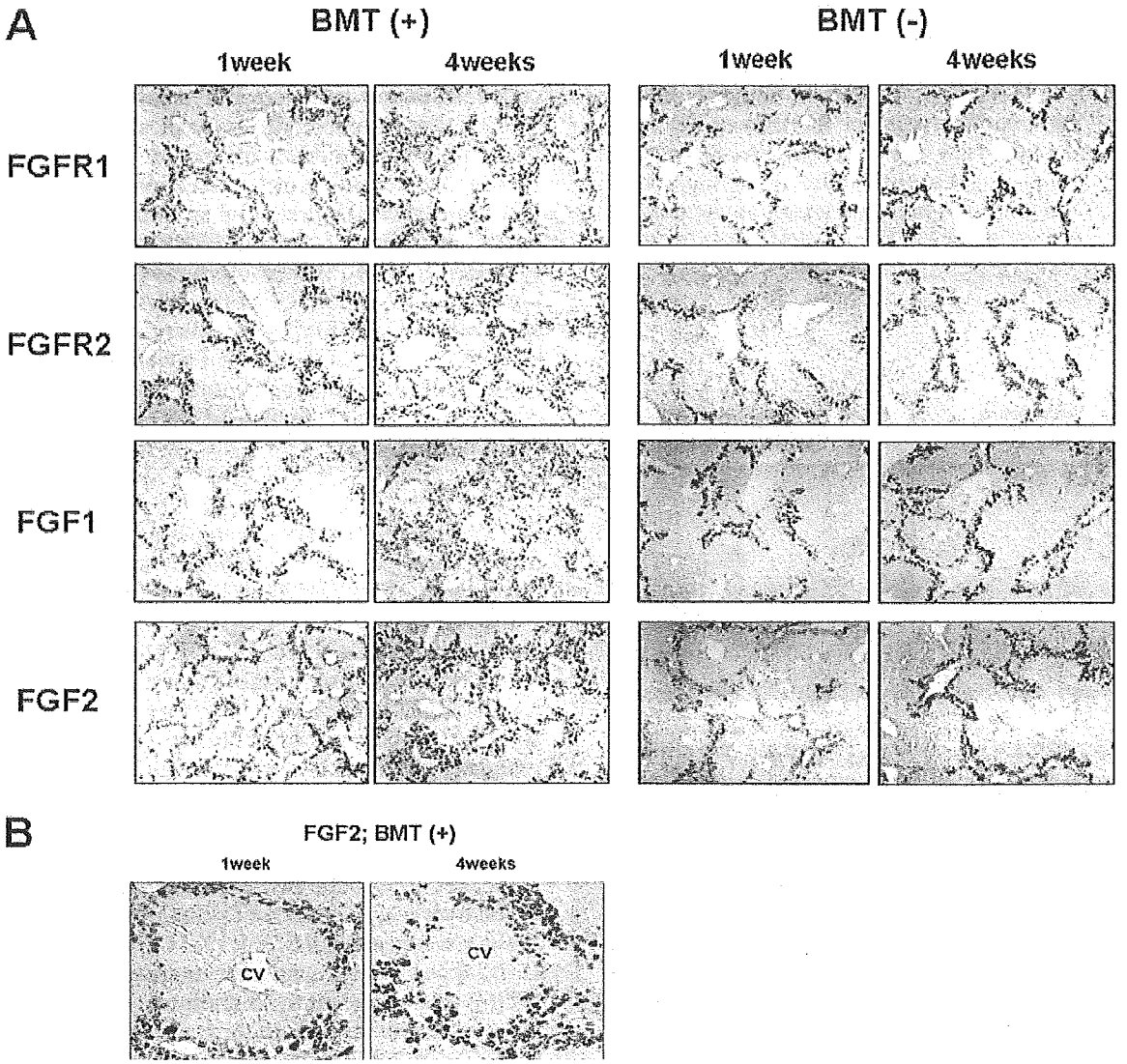

Fig. 2 Expression of FGFRs and FGFs (*BMT(+)* BMC transplantation group with CCl_4-induced persistent liver damage, *BMT(−)* control CCl_4-induced persistent liver damage group without BMT). One week (*1week*) in BMT(−) group represents 5 weeks of CCl_4 injection, and four weeks (*4weeks*) in BMT(−) group represents 8 weeks of CCl_4 injection. **A** Immunohistochemistry of FGFR1, FGFR2 and FGF1, FGF2 in BMT(+) and BMT(−) groups. In the BMT(+) group, the expression of FGFRs and FGFs significantly increases with time as compared with the BMT(−) control group, and the distribution of the proteins eventually extends from the peri-portal area into the intra-lobule. ×40 **B** Typical higher magnification image of FGF2 immunohistochemical staining in BMT(+) group. FGF2-positive cells proliferate and spread from the peri-portal area into the central area with time after BMT (*CV* central vein). ×200

Statistical analysis

Values are shown as means±SD. Data were analyzed with Fisher's exact test. A P-value of <0.05 was considered statistically significant.

Results

Expression of FGFRs significantly increases with time after BMT

For screening, we performed immunohistochemical staining with ten different antibodies recognizing growth factor receptors in the GFP/CCl_4 model. As shown in Fig. 1a,b, the percentage of stained area for FGFR1 and FGFR2 gradually and significantly increased each week after BMT ($P<0.05$). On the other hand, the expression of other growth factor receptors (c-Met, EGFR, VEGFR1/2, PDGFR α/β, and TGFβR 1/2) could be detected, but no significant chronological change in the expression level after BMT was found (Fig. 1c–j). These results suggest that FGF-FGFR signaling is most closely related to the process of BMC differentiation into hepatocytes in our model.

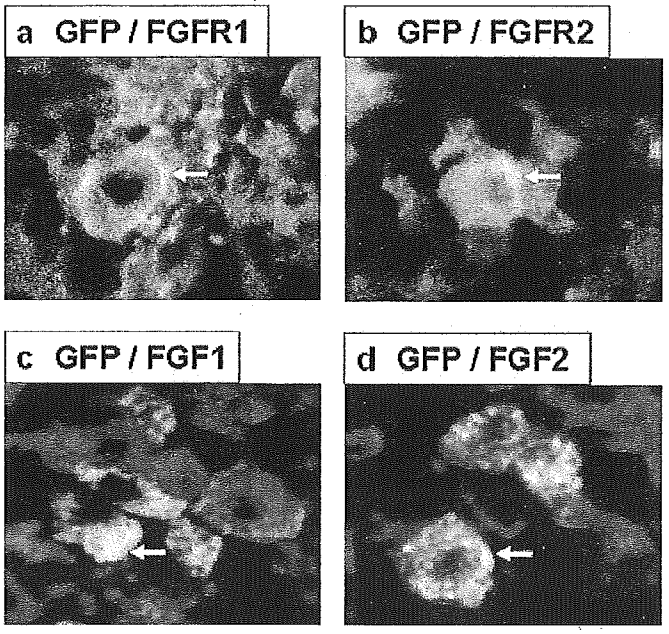

Fig. 3 Co-expression of GFP and FGFRs or FGFs in GFP/CCl_4 model. FGFRs are detectable at the cell surface of GFP-positive cells, and FGFs are detected in the cytoplasm of GFP-positive cells. Double-fluorescent merged images (*arrows* co-expression regions). **a** GFP (*green*), FGFR1 (*red*), co-expression of both GFP and FGFR1 (*yellow*). **b** GFP (*green*), FGFR2 (*red*), co-expression of both GFP and FGFR2 (*yellow*). **c** GFP (*green*), FGF1 (*red*), co-expression of both GFP and FGF1 (*yellow*). **d** GFP (*green*), FGF2 (*red*), co-expression of both GFP and FGF2 (*yellow*). ×400

Transplanted BMCs express FGFs and FGFRs during differentiation into hepatocytes

We further analyzed the expression of FGF1 and FGF2 and their receptors, FGFR1 and FGFR2, in the BMT(+) and BMT(−) groups. As shown in Table 1, BMT significantly elevated the percentage of the stained area of FGFRs and FGFs with time as compared with the BMT(−) control group ($P<0.05$). Furthermore, for each protein, the "percentage change" over time in the BMT(+) group was higher than that in the controls. Another obvious difference between the two groups was the distribution of the stained regions. Expression of FGFs and FGFRs was not detectable in the livers of normal mice (data not shown). In the BMT(−) group, expression of FGFs and FGFRs could be detected but consistently remained localized only to the peri-portal area. In contrast, in the BMT(+) group, expression of FGFs and FGFRs appeared to be up-regulated relative to control group, and the distribution of the proteins eventually extended from the peri-portal area into the intra-lobule (Fig. 2A). For example, the typical enlarged image of FGF2 immunohistochemical staining is shown in Fig. 2B. FGF2-positive cells proliferated and spread from the peri-portal area into the central area with time after BMT. To determine whether FGFs and FGFRs were detectable in the transplanted BMCs themselves, we analyzed the co-expression of GFP and FGFs or FGFRs. As shown in Fig. 3, co-expression of GFP and FGFRs was detectable at the cell surface. In addition, GFP and FGFs were both detected in the cytoplasm. These results indicate that transplanted BMCs express both FGFs and FGFRs during differentiation into hepatocytes.

FGF2 significantly elevates the repopulation rate of GFP-positive cells in the liver and increases the expression of both Liv2 and albumin

We investigated the effect of rFGF treatment on the process of the differentiation of BMCs into hepatocytes. In each group (BMC group, BMC+rFGF1 group, and BMC+rFGF2 group), the number of GFP-positive cells in the liver gradually increased after transplantation. GFP-positive cells were first detected in the peri-portal area and then in liver lobules with actively forming hepatic cords, suggesting a gradual spread into that region of the liver (Fig. 4A). In the BMC+rFGF1 group, the percentage of GFP-positive cells in the liver was 7.7±1.1% (1.4-fold more than in the BMC group) at 1 week, and 9.7±1.1% (1.2-fold more than in the BMC group) at 4 weeks after transplantation. The BMC+rFGF2 group showed the highest rate of liver repopulation among the three groups with a significant difference ($P<0.05$): 8.7±1.2% (1.6-fold more than in the BMC group, 1.1-fold more than in the BMC+rFGF1 group) at 1 week, and 10.7±1.2% (1.3-fold more than in the BMC group, 1.1-fold more than in the BMC+rFGF1 group) at 4 weeks after transplantation (Fig. 4B). The percentages of Liv2- and albumin-stained areas are summarized in Table 2. Treatment with rFGF, especially rFGF2, in combination with BMT

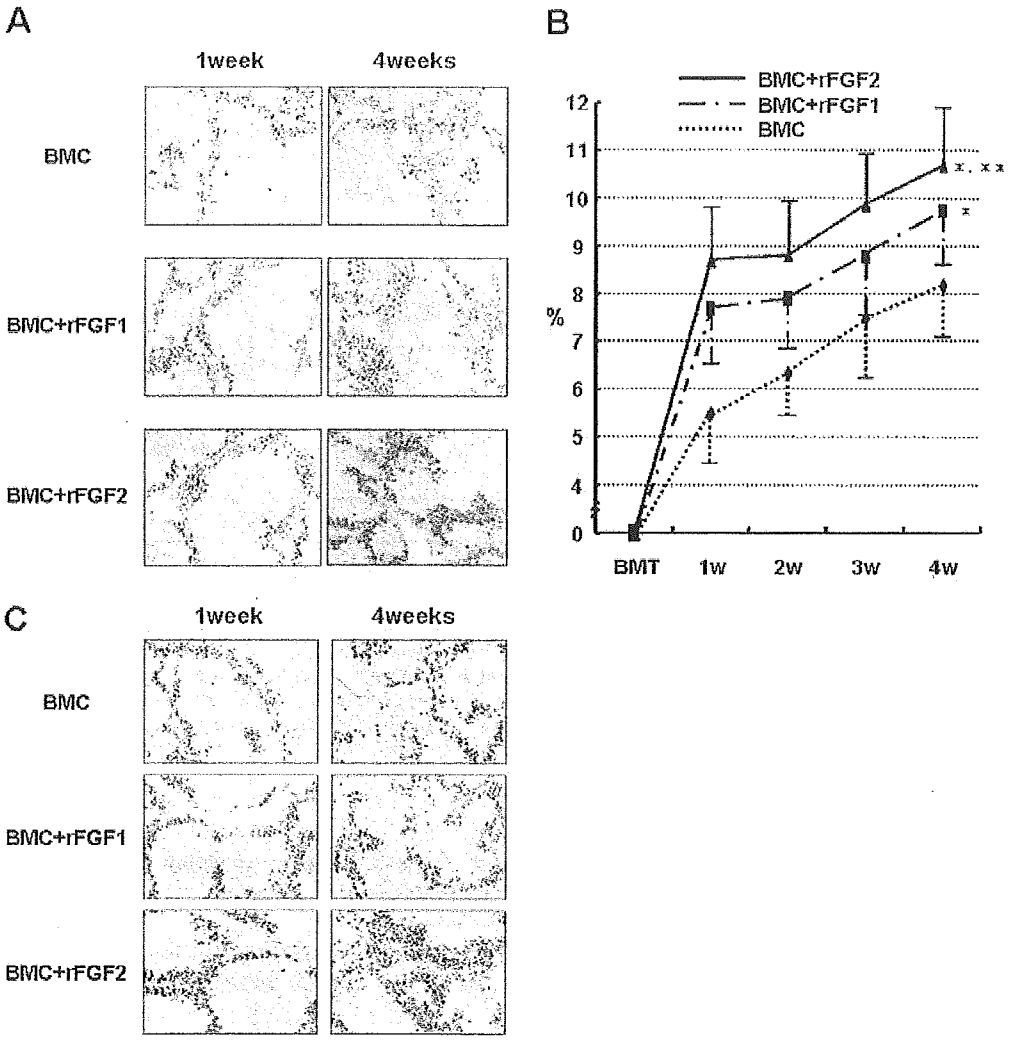

Fig. 4 Expression of GFP and Liv2 in BMC, BMC+rFGF1, and BMC+rFGF2 groups (*BMC* BMC-only transplantation without rFGF treatment *BMC+rFGF1* treatment with both BMCs and rFGF1, *BMC+rFGF2* treatment with both BMCs and rFGF2. **A** Immunohistochemistry for GFP. GFP-positive cells in the liver gradually increase and spread from the peri-portal area into the intra-lobule with actively forming hepatic cords in each group. The level of GFP expression in the BMC+rFGF2 group is the highest amongst the three groups. ×200. **B** Time-course of the percentage of GFP-positive cells in the liver. The BMC+rFGF2 group shows the highest percentage of stained area of GFP among three groups. *Significant difference compared with the value at same period in BMC group ($P<0.05$). **Significant difference compared with the value at same period in BMC+rFGF1 group ($P<0.05$). **C** Immunohistochemistry for Liv2. The distribution of Liv2-positive cells in the liver is similar to that of GFP-positive cells, and the level of Liv2 expression in the BMC+rFGF2 group is the highest amongst the three groups. ×200

Table 2 Percentage area stained immunohistochemically for Liv2 and albumin

Protein	Treatment	One week	Four weeks
Liv2 (hepatoblast marker)	BMC[a]	5.4%±0.9	6.0%±0.7
	BMC+rFGF1[b]	6.0%±0.6[c]	6.8%±0.9[c]
	BMC+rFGF2[d]	6.3%±0.8[c]	7.2%±0.9[c, e]
Albumin (hepatocyte marker)	BMC	11.1%±1.0	12.1%±1.0
	BMC+rFGF1	11.9%±0.9[c]	13.1%±1.0[c]
	BMC+rFGF2	12.1%±0.8[c]	13.6%±0.9[c, e]

[a]*BMC* BMC-only transplantation without rFGFs
[b]*BMC+rFGF1* Treatment with both BMCs and rFGF1
[c]Significant difference compared with the value at the same period in BMC group ($P<0.05$)
[d]*BMC+rFGF2* Treatment with both BMCs and rFGF2
[e]Significant difference compared with the value at the same period in BMC+rFGF1 group ($P<0.05$)

significantly increased the expression of both Liv2 and albumin compared with the BMC-only group ($P<0.05$). Moreover, the distribution of Liv2-positive cells in the liver was similar to that of GFP-positive cells (Fig. 4C). On the other hand, we could not detect Liv2 expression in either the rFGF1 group or the rFGF2 group without BMT (data not shown). Thus, FGFs, especially FGF2, are likely, directly or indirectly, to facilitate the ability of transplanted BMCs to populate the liver and to differentiate into hepatocytes via hepatoblast intermediates.

Administration of rFGF2 in combination with BMT significantly elevates serum albumin level and survival rate of mice with damaged liver

Next, we focused on FGF2 and further analyzed the effect of rFGF2 treatment with BMT. We compared serum albumin levels and survival rates for four groups: CCl_4 group, rFGF2 group, BMC group, and BMC+rFGF2 group (Fig. 5A,B). BMT itself significantly elevated both values compared with those of the control CCl_4 group ($P<0.05$), and BMT and rFGF2 treatment together resulted in serum albumin levels and survival rates that were significantly the